NTNU

Norwegian University of
Science and Technology

Investigation into the Capabilities of Linear Theory for Numerical Modelling of Wave-Body Interactions for a 2D Heaving Buoy

Application to Wave Energy Converters

David Short

Marine Technology
Submission date: June 2017
Supervisor: Trygve Kristiansen, IMT

Norwegian University of Science and Technology
Department of Marine Technology

PREFACE

The presented report comprises a master's thesis for the MSc degree program: Marine Technology with Specialisation in Hydrodynamics, offered by the Norwegian University of Science and Technology, accounting for 30 ECTS credits registered under the course code TMR4930 at the Department of Marine Technology. Work is original to the author and has been completed with the intention of increasing awareness regarding the capabilities of current state of the art numerical modelling techniques employed within the wave energy field, with a specific focus on heaving buoy type wave energy converters (WECs).

On a personal note, I would like to make several acknowledgements. To my project supervisor, Trygve Kristiansen, without who the thesis would not have been possible. He has provided constant guidance and motivation in addition to passionate explanations of theoretical hydrodynamics which have sparked many interesting discussions and topic extensions. To the SINTEF Ocean team, who were critical to the experimental work that has been undertaken, I would like to express my huge gratitude. Particularly to Trond Innset who was responsible for model construction and to Torgeir Wahl, Terje Rosten, Ole Erik Vinje and Marcus Johnsen Almehagen who contributed to the experimental set-up and operation. To Joao Cruz and Tiago Martins of Cruz Atcheson consulting engineers, for helping to establish a field of interest for the project and providing the structural geometry that has been analysed. Their early contributions were fundamental to my understanding of the numerical modelling techniques utilised within the WEC sector. To Jarle Kramer and Tufan Arslan, for sharing with me some of their extensive knowledge regarding computational fluid dynamics and helping me to overcome many numerical modelling hurdles during the presented project.

Last but not least, I would like to take the opportunity to thank my loved ones who have been tirelessly supportive throughout my time at university and have encouraged me to follow my interests.

Trondheim, June 2017

David Short

SUMMARY

Numerical modelling of wave energy converters (WECs) is currently an area of interest within the marine renewable energy industry, due to its ability to streamline design processes and accelerate scientific understanding. The presented project investigates the capacity of linear potential flow theory to accurately model wave excitation of a 2D WEC buoy-section, identifying wave conditions under which computational fluid dynamics (CFD) become a more appropriate strategy.

OpenFOAM® v1612+ is utilised to simulate fully non-linear, viscous wave-structure interactions for comparison with linear theory and experimental results. Regular waves are generated to study both fixed and floating body cases.

Linear forces are compared with those computed during fixed body CFD simulations, the validity of which is investigated using wave flume experiments carried out in NTNU's Ladertanken wave flume facility. Experimental and numerical results show reasonable agreement. 1st harmonic CFD forces compare well with linear forces in cases where overtopping is not observed. 2nd harmonic loads are shown to have significant contributions to total forces.

Floating body CFD simulations are carried out allowing heave response displacements to be obtained for comparison with linear theory predictions. For the tested cases, responses are dominated by 1st harmonics, making comparison with linear theory particularly interesting. Good agreement is seen between linear theory and CFD for wave frequencies far from the natural frequency in heave, however divergence is seen for steep waves close to resonance where overtopping is extensive.

CONTENTS

LIST OF FIGURES

LIST OF TABLES

1 INTRODUCTION

1.1 BACKGROUND AND MOTIVATION

With the world looking towards alternative energy solutions following the 1974 oil crisis, the first serious scientific attention was paid to harnessing the power of ocean waves. Numerical modelling techniques became vital in improving wave energy convertor (WEC) designs that had previously been based solely on analytical estimations, intuition and empirical experience. Such tools, many of which are still used today, aim to model wave-body interactions via predicting induced loads and structural responses.

Since the 1970s, a variety of wave energy converter (WEC) concepts have emerged along with a plethora of numerical modelling techniques. WECs can be split into 3 main categories; oscillating water columns, overtopping devices and oscillating bodies, all of which may be fixed or floating structures. Oscillating water columns use wave elevation to compress air inside a chamber which in turn runs a bi-directional turbine generator, overtopping devices allow water to flow into a reservoir past conventional hydro turbines, while oscillating bodies, also called wave activated bodies, respond directly to wave motion, generating electrical power through power take off systems such as hydraulic actuators.

The majority of marine hydrodynamic modelling techniques evolved to analyse offshore structures such as ships and oil platforms, but have since been applied to and adapted for WECs. (Folley, 2016) describes that up until 1997 all numerical models of WECs were based purely on linear potential flow theory and that today 90% still are. WAMIT, developed by Chang-Ho Lee and John Newman in 1987, is a commonly used wave-structure interaction code based primarily on linear theory, utilising a boundary element method (BEM) to solve potential flow problems in the frequency domain, offering fast computation times and results that have been validated extensively for a range of applications.

As the WEC sector has developed the need for second generation design tools, capable of analysing nonlinear fluid effects commonly experienced under extreme wave conditions, has become apparent. Techniques that capture nonlinear effects are prevalent within the marine

industry, these include, weakly non-linear frequency domain methods based on expanding the perturbation series from which linear potential theory is derived, partially non-linear time domain approaches such as ACHIL3D, fully non-linear time domain potential flow codes as well as computational fluid dynamics (CFD), which possesses the ability to model fully nonlinear viscous flow problems.

A key challenge for the wave energy industry is to identify which numerical modelling techniques are most appropriate for each WEC design under specific environmental conditions. This is made particularly difficult due to the diversity in energy generation processes and the variety in wave characteristics to which WECs are exposed. For example, the most appropriate method for analysis of a WEC in its power production operational state, in which only small waves are present, is likely to be unsuitable for its survival mode in which it is exposed to severe sea states. Design tools based on fully non-linear methods are generally required for the latter, however it is of interest to examine to what extent simpler potential flow methods are acceptable for analysis of each WEC design. The presented project aims to contribute to the knowledge base regarding this topic for WECs that utilise heaving buoys to generate electrical power, such as point-absorbers (PAWECs) and floating oscillating water columns (FOWCs). (Ye Li and Yi-Hsiang Yu, 2012) describes PAWECs as one of the most cost-efficient technologies and that no one modelling method has been recognised as superior for all scenarios. Whilst having many advantages in terms of computational cost, weakly nonlinear frequency domain potential flow methods, based fundamentally on linear theory, cannot produce accurate results for a number of key situations in which viscous and non-linear wave effects are prevalent. It is therefore important to thoroughly explore linear theory's capabilities regarding the estimation of wave induced forces and responses for heaving buoys such that these methods can be used both safely and effectively.

1.2 CONTRIBUTION

To aid in the development of PAWECs and FOWCs, linear theory's capacity to model wave excitation of floating buoys is explored, with the main objective to investigate under which regular wave characteristics non-linear effects become substantial for a 2D heaving buoy, providing an indication of the limitations of current state of the art numerical modelling tools that are based on linear theory. For this, two main procedural steps are defined as follows:

1. Analyse linear theory's performance in computing wave-induced vertical forces on a fixed buoy by comparing linear theory with both experimental and CFD results. Specifically, assess 1st harmonic loads with reference to linear forces and evaluate the magnitude of higher order contributions.

2. Analyse linear theory's performance in predicting wave-induced heave responses of a floating buoy section by comparing linear response amplitude operators with those of CFD simulations.

1.3 SCOPE

Fixed cases simulations in procedural step 1 and floating case simulations in step 2 are performed using the open source CFD toolbox, OpenFOAM® v1612+. Regular waves of steepness 1/60, 1/45, 1/30 and 1/15, defined as wave height, H, divided by wave length, λ, are tested for 0.8, 1.0 and 1.2 second periods in both cases, providing a large variety of conditions under which linear theory is examined. Experimental replication of the fixed case simulations is performed to assess the validity of numerical results.

Vertical forces and motions are examined as they are of great significance to the power production of heaving buoy type wave energy converters. Horizontal effects are not considered.

The 2D cross section of a cylindrical buoy is analysed, belonging to a FOWC design provided by Cruz Atcheson Consulting Engineers. A 3D approach has not been considered due to the extensive computational requirements involved.

1.4 REPORT STRUCTURE

The remainder of the report is organised as follows

- **Chapter 2** identifies physical characteristics and phenomenon associated with wave excitation of marine structures related to heaving buoy type WECs and describes the fundamental principles of numerical modelling based on potential theory and CFD.
- **Chapter 3** provides the details of the presented problem, defining a coordinate system and describing the structural geometry.
- **Chapter 4** details the experimental method used to obtain wave induced vertical forces on the fixed WEC buoy structure.
- **Chapter 5** describes the numerical method employed for fixed and floating case simulations. Results from sensitivity studies used to determine computational parameters are presented at this stage. The chapter goes on to outline the linear force and response calculation procedure as well as specifying the post-processing techniques utilised throughout the project.
- **Chapter 6** presents results and provides discussion of linear theory's performance in the given cases.
- **Chapter 7** draws conclusions from the project.
- **Chapter 8** offers recommendations for future work.

2 WAVE EXCITATION OF OFFSHORE STRUCTURES

Heaving buoy type WECs installed in ocean environments are constantly exposed to waves with a large range of characteristics causing loads and responses of varying severity, in which linear and non-linear effects are present. The following chapter examines a selection of these effects and provides a brief explanation of numerical modelling techniques that are commonly used to capture them. As stated by (Henry et al., 2013), there is currently a "lack of empirical load data for wave energy converters, therefore knowledge and guidance must be drawn from other industries", thus examples of wave excitation shall also be given regarding structures that relate closely to heaving buoy type WECs.

2.1 HARMONIC WAVE LOADING

As with all cyclical type loading, the total wave force experienced by a structure may be decomposed into its 1st and higher-order harmonic contributions, oscillating at integer multiples of the applied loading frequency. 1st harmonic forces are in phase with the fundamental frequency and are referred to as linear forces. In theory for low wave steepness one expects the 1st harmonic to completely dominate and thus the system behaves linearly. For high steepness waves the 2nd, 3rd and in some cases higher-order harmonics may carry a significant proportion of the total energy, inducing non-linear effects. In theory, potential flow methods are sufficient to model wave harmonics, as such wave effects are purely inertial. Linear codes have the ability to capture 1st harmonic force, however higher order contributions require non-linear modelling.

The importance of higher harmonic behaviour is recognized throughout the marine industry. A typical example is for tension-leg platforms (TLPs), whose natural periods are generally between 1-4 seconds and are thus outside the appreciable incident energy spectrum but may be excited by the 2nd harmonic, as stated by (Kim, 1991). This may be in the form of springing, an oscillatory response caused by wave effects at sum frequencies (the 2nd harmonic), described thoroughly by (Srinivasan et al., 2011). Wind turbine foundations are composed of asymmetrical vertical cylinders similar to TLPs and can also experience

significant loading caused by higher-order harmonics. (Paulsen et al., 2014) explores the phenomenon of ringing, observed as a strong transient response triggered by large wave impacts. This is often attributed to the third harmonic force. Higher-harmonic load effects are also of key concern in the design of large slender hulled vessels; (Hänninen et al., 2016) explains the development of second harmonic springing loads on a large cruise ship. Modelling of high order harmonics is achieved either through nonlinear potential flow methods or using CFD.

2.2 WAVE BREAKING AND VISCOUS LOADS

Wave breaking here refers to overtopping and slamming caused by the presence of a body. Such effects are common when structures are exposed to waves of significant height as well as during significant body motion, for example when resonance occurs. Overtopping and slamming loads are highly non-linear in nature but as they are generally initiated in phase with the wave frequency they can have influence over 1st harmonic forces and response. Wave breaking requires highly accurate free-surface modelling and thus potential flow methods in which the free-surface is not discretized are insufficient. A common approach is to use surface capturing techniques such as the volume of fluid (VOF) method in combination with two phase CFD.

Viscous forces arise primarily from flow separation within the boundary layers of offshore structures. This is caused by adverse pressure gradients caused by variation in body form, for example at sharp edges and along curved surfaces. Such effects may only be modelled by solving the Navier Stokes equations, which govern viscous fluid flows, using computational fluid dynamics (CFD), as described in the following section.

2.3 NUMERICAL MODELLING

As hinted at in the introduction, there are two main schools of thought when it comes to numerical analysis of complex geometries within the marine hydrodynamics field. The first was born with the introduction of computers for engineering applications in the late 20th century, where numerical tools for hydrodynamic analysis of marine structures were developed based upon linear potential flow theory. Such tools show good agreement with experimental data for a wide range of applications and are highly valuable to the industry. Progress has been made in applying nonlinearity to potential flow models for many applications.

As computational power has evolved new solution techniques have been developed, designed to model more thoroughly the physics of engineering problems. The second accepted norm relating to numerical marine hydrodynamics revolves around the use of such techniques to solve the fully non-linear Navier-Stokes (NS) equations, which model viscous fluid behaviour. There are no analytical solutions to the NS equations; they must be solved iteratively with numerical schemes. This process is known generally as computational fluid dynamics (CFD).

The present section addresses the fundamental background to both potential flow methods and CFD as well as offering insight into the current state of numerical analysis for heaving buoy type wave energy convertors and related structures.

2.3.1 Potential flow methods

A potential or ideal flow is assumed to be incompressible (i.e. with constant density), irrotational (i.e. without vorticity) and inviscid (i.e. without viscosity). The need for mass continuity in a flow of constant density leads to the following equation,

$$\nabla^2 \varphi = 0$$

Where,

- φ: Velocity potential
- ∇: Gradient operator

This is known as the Laplace equation and governs potential flow. Applying appropriate boundary and initial conditions, for a given engineering situation, on a domain governed by Laplace allows a boundary value problem (BVP) to be formulated in which the velocity potential, φ, can be found.

The boundary conditions required for marine engineering problems comprise of; a kinematic condition, established on the bottom boundary such that water does not flow through it; a similar body impermeability condition ensuring no flow through the structure; a kinematic free-surface boundary condition to ensure that fluid particles on the free surface remain there; a dynamic free-surface condition prescribing fluid pressure to be equal to the ambient (atmospheric) pressure along the free surface and finally for a radiation condition in which waves are considered to be outgoing meaning that velocities tend to zero far from the body.

In describing BVPs, the level of wave non-linearity captured by the model may be controlled. Fully non-linear models apply boundary conditions on the instantaneous free surface and wetted body. This is a demanding process and requires significant coding specific to a given geometry and problem. More commonly linear and weakly non-linear approaches are used in which the velocity potential, φ, is expressed in terms of a power series in some parameter, ε, measuring the non-linearity in the system. This is known as a perturbation expansion and is shown below.

$$\varphi = \widetilde{\varphi_1}\varepsilon + \widetilde{\varphi_2}\varepsilon^2 + \widetilde{\varphi_3}\varepsilon^3 \ldots . = \varphi_1 + \varphi_2 + \varphi_3 \ldots.$$

Where,

- φ_1: First order solution for velocity potential; proportion to ε
- φ_2: Second order solution for wave elevation; proportion to ε^2

Etc.

The main source of non-linearity in marine problems enters due to wave steepness thus the parameter commonly used is

$$\varepsilon = {\zeta_a}/{\lambda}$$

For linear and weakly non-linear methods, boundary conditions are applied at the mean free-surface and the mean wetted body rather than the instantaneous levels. This is achieved using Taylor series expansions around $z = 0$. By substituting the perturbation series into the governing equation and boundary conditions and retaining terms of a desired level of non-linearity BVPs may be formulated for each solution order. Numerical approaches require discretization of these boundaries into finite elements for which individual solutions may be found.

In solving linear potential flow theory, a description of the velocity potential which satisfies the linearized boundary conditions is found. Methods based on such formulations can be used to model 1st harmonic wave loads which oscillate at the wave's fundamental frequency. A solution for wave elevation may be found using the computed linear velocity potential in the dynamic free-surface boundary condition, this results in regular sinusoidal wave forms which replicate small steepness ocean waves. Under linear theory, forces induced by waves with constant length but varying amplitude can be calculated simply by scaling one known solution proportionally to the desired amplitude. However, an error exists within Linear theory as it assumes constant velocity potential between the mean free-surface and the free-surface level, meaning that under the wave trough hydrostatic and dynamic pressure do not cancel each other as required in the dynamic free-surface boundary conditions. This is of greater significant at high wave steepness and must be considered when scaling up forces.

Weakly nonlinear methods solve both the linear and higher order boundary value problems. Through retaining higher order terms, the boundary conditions are more accurately satisfied and thus more of the physics occurring within the problem is modelled. Such methods have the ability to model the higher order harmonic contributions contained within wave loads. A 2nd order method based on perturbation expansions can in theory model the 2nd harmonic, a 3rd order formulation will resolve the 3rd harmonic and so on. Wave elevation results from weakly nonlinear methods effectively imitate the observed forms of ocean waves with steepness greater than those modelled by linear theory.

Figure 1 below shows the wave characteristics that linear and weakly nonlinear potential flow theories can accurately model. Regions have been calculated by solving perturbation expansion BVPs without the presence of structural bodies.

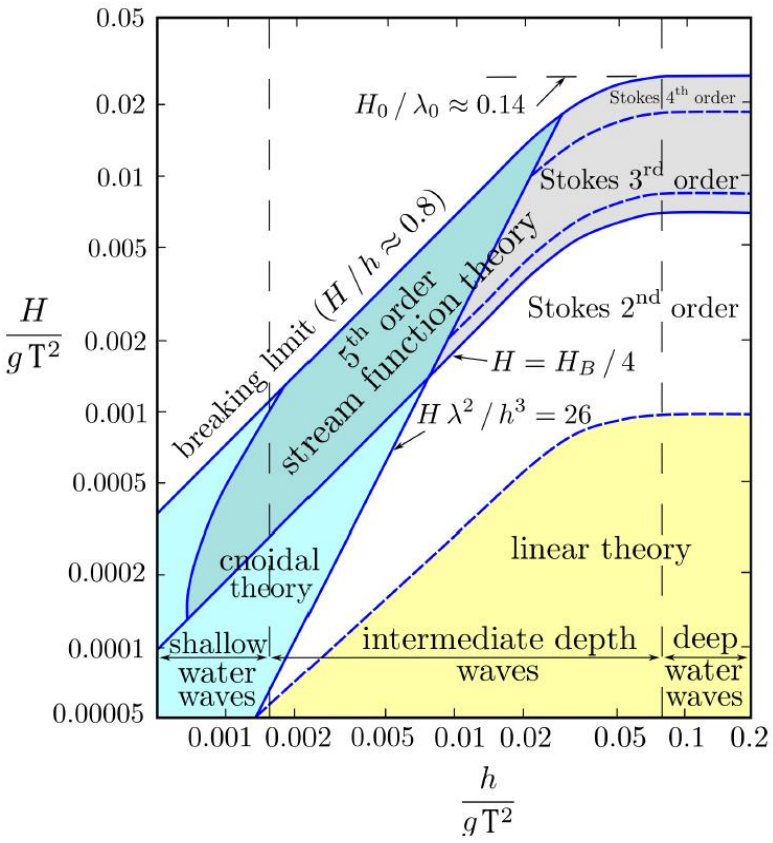

Figure 1. Ranges of applicability for potential wave theories. Taken from (Le Mehaute, 2013)

For all potential flow calculation, the acquired function φ is unique to the given engineering problem and can be used to find fluid velocities as well as pressure using Bernoulli's equation,

$$p = p_a - \rho g z - \rho \frac{\partial \varphi}{\partial t} - \frac{1}{2}\rho(\nabla\varphi)^2$$

With,

- ρ: Fluid density
- p_a: Ambient pressure
- $-\rho g z$: Hydrostatic pressure
- $-\rho \frac{\partial \varphi}{\partial t}$: Linear dynamic pressure
- $-\frac{1}{2}\rho(\nabla\varphi)^2$: Non-linear pressure term, which is disregarded when computing pressure under linear theory.

In weakly non-linear approaches, non-linear pressure terms are included once again through inserting perturbation expansions and retaining the desired higher order terms. Pressure forces on a marine structure can then be found simply by integrating the pressure over the its wetted surface as

$$\boldsymbol{F} = -\int_{S_B} p\boldsymbol{n}dS$$

Where,

- S_B: Wetted body surface
- $\boldsymbol{n}$: Unit normal vector to the body surface, where positive direction is defined to be into the fluid.

To analyse a floating structure's seakeeping performance in waves using potential flow theory, two problems must be solved. Firstly, a diffraction problem in which the structure is fixed and the loads exerted on it by waves, known as excitation forces, are calculated.

Excitation forces exerted on a fixed structure can be split into two categories, namely Froude-Krylov and diffraction forces. Froude-Krylov forces can be considered as the result of the flow associated with the incident wave trying to penetrate the structure with normal velocity, $\frac{\partial \varphi_o}{\partial n}$, where φ_O is the velocity potential of the incident wave. To ensure body impermeability the body presence causes a flow which can result in diffraction waves, described by the velocity potential φ_D. This flow causes hydrodynamic loads, due to dynamic pressure changes on the body, called diffraction forces. Excitation forces are therefore given by

$$\boldsymbol{F_{exc}} = -\int_{S_B} p_{dO}\boldsymbol{n}\, dS - \int_{S_B} p_{dD}\boldsymbol{n}\, dS$$

Where,

- p_{dO}: Dynamic pressure associated with incident wave velocity potential

- p_{dD}: Dynamic pressure associated with velocity potential of the diffracted flow

The first term on the right-hand side of the equation represents Froude-Krylov forces. The second term represents diffraction forces.

Secondly, a radiation problem where the structure is given a prescribed motion and forces induced by the fluid on the structure are calculated. The problem is solved to find a velocity potential for the radiated flow, expressed as, φ_R. Radiation forces can then be calculated as

$$\boldsymbol{F_{rad}} = -\int_{S_B} p_{dR}\boldsymbol{n}\, dS$$

Radiation forces in phase with the body's acceleration are known as added mass forces and those in phase with its velocity are wave damping forces. In uncoupled heave motion the radiation forces are given by

$$F_{rad,3} = -A_{33}\ddot{\eta}_3 - B_{33}\dot{\eta}_3$$

Where,

- A_{33}: Added mass coefficient in heave due to heave motion
- B_{33}: Wave damping coefficient in heave due to heave motion

Such forces are dependent on body form and frequency of the applied oscillatory motion.

The response of the floating structure to waves may then be found using Newton's second law of motion

$$m\ddot{\boldsymbol{\eta}} = \sum \boldsymbol{F} = \boldsymbol{F_{exc}} + \boldsymbol{F_{rad}} + \boldsymbol{F_{rest}}$$

$\boldsymbol{F_{rest}}$is the restoring force vector caused by changes in buoyancy experienced during body motion. For small amplitude uncoupled heave motion, in which the WPA remains constant, $F_{rest,3}$ may be expressed as

$$F_{rest,3} = -C_{33}\eta_3$$

Where,

- C_{33}: Linear restoring force coefficient in heave due to heave motion, computed as

$$C_{33} = \rho g WPA$$

- η_3: Heave displacement

The equation of motion for uncoupled heave motion may then be formulated from Newton's second law as

$$(m + A_{33})\ddot{\eta}_3 + B_{33}\dot{\eta}_3 + \rho g WPA\eta_3 = F_{exc,3}$$

Where,

- $\dot{\eta}_3$: Heave velocity
- $\ddot{\eta}_3$: Heave acceleration

If radiation forces are known for the excitation force frequency then the heave response, η_3 , can be computed by solving the ordinary differential equation above. Occasionally additional terms are included in the equation of motion to model some level of viscosity in the problem based on empirical expressions. With constant coefficients, the equation of motion may be solved in the frequency domain. On the other hand, if parameters vary as the body is excited the equation of motion must be solved in the time domain, i.e. solutions are computed at each time step in an iterative process. Partially non-linear time domain approaches utilise linear and weakly non-linear potential formulations for computing hydrodynamic forces but are solved in the time domain for the treatment of time dependent terms, such as time varying restoring forces; for floating non-moored bodies this can be caused by changes in wetted body form during motions. Fully non-linear methods follow a similar approach but solve BVPs with boundary conditions applied at instantaneous surfaces and require approaches in which the free-surface position and wetted body form is updated at each time step.

A sizeable proportion of numerical software utilised in the marine industry use linear and weakly non-linear potential flow formulations to find velocity potential and perform frequency domain calculations to model floating interactions. WAMIT, developed by Chang-Ho Lee and John Newman in 1987, and ShipX, created by MARINTEK in the late 1990s, are examples of such interaction codes. WAMIT is based on first and second order potential flow theory, utilising perturbation expansions of boundary conditions and pressure expressions. In modelling wave excitation of a floating structure WAMIT first solves a radiation problem where the body is forced to oscillate at the same frequency as the incident waves that it will subsequently be exposed to. Here the added mass and damping coefficients are obtained. A diffraction problem is then solved to calculate excitation forces and the equation of motion is solved in the frequency domain, producing a time series of the body's response. Tools like WAMIT utilise BEMs, also called Panel methods, in which the mean wetted body boundary is discretized into a finite number of sections. Green's function, given as equation (4.25) in (Faltinsen, 1993), is then applied to each section, describing a solution for φ represented by surface distributions of singularities over the discretised elements. The function is known to satisfy the environmental boundary conditions describing the domain of a linear potential free-surface flow problem. A solution is established by assigning strength factors to each singularity corresponding to the body's boundary condition, a negative factor indicating a sink and a positive factor describing a source. The solutions for velocity potential are used to compute hydrodynamic forces within the radiation and diffraction problems. Green's functions are only used to solve linear problems but can be coupled with higher order solutions found from perturbation methods. One of the key advantages of such linear and weakly non-linear potential flow tools is that solutions only need to be found on the mean body and free-surface boundaries, thus there is no need to discretize the surrounding fluid. In the case of linear solutions using Green's functions only the mean body boundary requires modelling. This coupled with frequency domain solution procedures leads to very fast analysis, requiring little computational power.

(Ye Li and Yi-Hsiang Yu, 2012) describes how weakly nonlinear frequency domain BEM approaches, based on perturbation expansions with boundary conditions specified at the mean free-surface and body surface, have been used successfully to solve wave radiation and diffraction problems for floating bodies. For example (Cruz and Salter, 2006) obtained hydrodynamic coefficients based on linear potential flow theory for a modified version of the

Edinburgh Duck WEC using WAMIT. Comparison of response predictions with experimental work showed good correlation away from resonance frequencies but poor correlation around natural frequency, confirming limitations of linear theory. (McCabe et al., 2007) employed WAMIT to find linear hydrodynamic coefficients in order to estimate response of axisymmetric bodies in waves, which relate closely to heaving buoy type WECs. Higher order potential flow methods have been employed for modelling wave induced forces on vertical cylinders like in (Newman, 1996), which captured second order harmonic loads. A fully non-linear approach has been utilised in (Bai and Taylor, 2006), successfully predicted non-linear irregular wave radiation of vertical cylinders. (Ferrant et al., 2003) managed to solve the diffraction problem in a similar way.

2.3.2 Computational fluid dynamics

CFD aims to solve the mathematical expressions for the conservation laws of physics that govern viscous fluid flow and thus theoretically it can describe the physical reality of fluid problems. For hydrodynamic applications, we are interested in accurately calculating fluid velocities and pressures exerted on marine structures by their environments. With this in mind, CFD provides the ability to model real flow physics, such as viscous forces, wave breaking loads and fully nonlinear inertial effects experienced during wave-body interactions. Thus, in certain situations correctly implemented CFD will provide velocity and pressure results with superior accuracy to potential flow methods. However, the process is computationally exhaustive and should only be used when such effects are critical to engineering problems.

Mesh based methods in which the fluid domain is discretised into control volumes are the most common CFD approaches and will be examined here.

The need for mass conservation of a fluid in a domain gives rise to the first governing equation of any CFD model: the continuity equation. In integral form the continuity condition for a single control volume Ω reads

$$\underbrace{\int_{\Omega} \frac{\partial \rho}{\partial t} dV}_{I} + \underbrace{\int_{\partial\Omega} \rho \boldsymbol{U} \cdot \boldsymbol{n}\, dA}_{II} = 0$$

Where,

- I: Rate of mass change inside control volume Ω
- II: Net mass flow over control volume boundary $\partial\Omega$
- $\boldsymbol{U}$: Velocity vector
- $\boldsymbol{n}$: Unit normal vector to the control volume boundary, where positive direction is defined out from the surface into the surrounding s fluid.

Water is almost perfectly incompressible meaning that density remains constant if the temperature is fixed, thus for marine applications the continuity equation becomes,

$$\int_{\partial\Omega} \boldsymbol{U} \cdot \boldsymbol{n}\, dA = 0$$

Newton's second law of motion must also be satisfied within the system, that is the rate of change of momentum in a system is equal to the sum of the forces exerted upon it. Mathematically in integral Newton's second law for a single control volume reads

$$\underbrace{\int_{\Omega} \rho \frac{\partial \boldsymbol{U}}{\partial t} dV}_{I} + \underbrace{\int_{\partial\Omega} \rho \boldsymbol{U}\boldsymbol{U} \cdot \boldsymbol{n}\, dA}_{II} = \underbrace{-\int_{\partial\Omega} p\boldsymbol{U}\, dA}_{III} + \underbrace{\int_{\partial\Omega} \underline{\boldsymbol{\tau}} \cdot \boldsymbol{n}\, dA}_{IV} + \underbrace{\int_{\Omega} \rho \mathbf{f}\, dV}_{V}$$

With,

$$\rho = constant$$

Where,

- I: Unsteady temporal term expressing rate of momentum change inside control volume Ω
- II: Convective term showing momentum flow over control volume boundary $\partial\Omega$
- III: Source term giving pressure force acting on control volume boundary $\partial\Omega$
- IV: Diffusive term showing viscous force acting on control volume boundary $\partial\Omega$
- V: Source term for external volume force on Ω
- $\underline{\boldsymbol{\tau}}$: Viscous stress tensor
- $\mathbf{f}$: External force vector

This equation which can be described as a general transport equation and provides the second governing equation for viscous incompressible fluid flows. It is known as the Navier-Stokes momentum equation and can be split into three separate transport equations, one for

each velocity component. A third governing equation for viscous flows exists expressing the first law of thermodynamics which describes conservation of energy in the system. For marine applications, we are generally not interested in modelling properties such as temperature variation in the fluid thus the third governing equation is not explored here. Velocities and pressure may be calculated using only the first and second governing equations.

The first step of any CFD calculation is always to discretize the solution domain into a meshed grid of control volumes, known as cells. The orthogonality of the grid should be considered as this can dramatically influence numerical performance. Meshes may be refined at points of interest were flow characteristics are likely to be more complex. To compute fluid flow variables on such a grid, CFD software such as OpenFOAM employs the finite volume method (FVM) in which the transport equations are conserved for each cell and thus transported quantities can be found at cell centroids. An advantage of FVM is that it allows for varied grids unlike the simpler finite difference method (FDM), thus control volumes can take any shape allowing CFD analysis within geometrically complex domains. One possible drawback is that FVM only has the capacity to model variation in a cell linearly unlike more complex methods like the finite element method (FEM).

Within FVM, transport equations are discretized for each cell using a variety of numerical schemes. It should be noted that as these are second order equations, CFD practitioners should aim to use second order or higher discretization schemes to help achieve good accuracy. Firstly, the convective and diffusive terms are reformulated using Gauss's theorem to convert volume integrals into surface integrals in a way that integration may be achieved by summing the fluxes at each cell face. Interpolation schemes are used to find the boundary flux values using centroid results. Such schemes should be selected with the aim of producing accurate non-oscillatory (bounded) solutions. Commonly however a balance must be struck between numerical stability and accuracy, as higher-order schemes are generally less stable. Total variation diminishing schemes help to reduce the oscillatory behaviour of higher order schemes and are generally an appropriate choice for convective fluxes. Source terms within transport equations are discretized into linear and non-linear contributions. This concept can model source terms exactly as long as they are constant or vary linearly with the transported quantity. Finally, the temporal term must be discretized. Again, many schemes exist, both implicit and explicit, with varying levels of stability and accuracy.

Turbulence must also be considered when setting up a CFD simulation. If turbulence were to be modelled completely the mesh would have to be refined down to the Kolmogorov length scale which represents the size of smallest possible eddy structure for the given flow. Solving the Navier Stokes equations directly with meshes at this scale is known as direct Navier Stokes (DNS) CFD, however this is impractical due to enormous computational requirements and is not considered for most cases. Instead a more common approach is Reynolds averaged Navier Stokes (RANS) CFD where average flow velocities are computed and additional transport equations are used to model turbulent fluctuations. RANS also includes specific treatment close to wall boundaries to estimate the effect of turbulent flow. Alternatively, if turbulent effects are deemed non-critical for a problem the Navier Stokes equations may be solved directly on a course grid, this is known as laminar modelling.

Once each transport equation has been discretized they are rearranged into systems of linear algebraic equations, stored as matrices, describing the transported variables across the entire domain. Boundary and initial conditions are applied and the system is solved either iteratively or directly. For wave body interaction problems, as in potential flow methods, impermeability conditions are required on the body and domain bottom. The free surface is not considered as a boundary but as an interface between two flows with distinct phases.

To model the free surface behaviour including wave breaking, interface capturing methods such as the volume of fluid (VOF) technique are a common choice. VOF uses phase fractions, α, to define the free-surface. In a general marine case; water has α equal to one and air is set to zero. Cells with a composition of water and air receive corresponding proportional alpha values between 0 and 1, this allows complex free-surfaces to be modelled without the need for a moving mesh, helping to reduce computational cost. A transport equation for α is established and treated in an analogous way to the NS momentum equation. The relative volume fraction of the two phases in each cell, α, can then be computed and used to express physical properties of the flow as weighted averages. With the free-surface established waves must be generated at an inlet boundary, a typical approach for this is prescribing fluid velocities at the boundary corresponding to the solutions of potential wave theories. Depending on the desired wave characteristics, the appropriate theory can be selected in accordance with le Mehaute's work presented in figure 1. (Zhao et al., 2010) investigated extreme wave generation using the VOF method and produced promising results.

A solution algorithm is required in which the method used for calculating pressure based on velocity results is defined. Generally, this is achieved using an iterative process in which initial values for velocity and pressure are prescribed through initial conditions. Intermediate velocity values are then computed by solving the momentum equation for the current time step. These values are then used in a pressure correction equation based on the 1st governing equation, before the pressure value is updated. Additional transport equations are then solved with the corrected pressure and velocity terms. This process is iterated until convergence, determined by set tolerances, in solutions is achieved before moving onto the next time step.

Finally, before simulations can be run a suitable time step should be selected. Alternatively, an adjustable time step can be used, controlled by a parameter known as the Courant or CFL number which describes the rate of information flow across a cell and has influences over accuracy and stability of calculations. For fluid motion in the x direction, it is defined as

$$C = \frac{u\Delta t}{\Delta x}$$

The courant number should be set to improve stability, and thus convergence, of numerical schemes. For stability of some, mostly explicit, temporal schemes a condition of $C < 1$ is required such that information does not traverse more than one cell per time step.

For marine applications in which structures response to wave-body interactions the body may be modelled in several ways. Immersed boundary methods can be used in which the fluid is given a Eulerian description with variables defined on fixed cartesian coordinates and the body boundary is defined by Lagrangian variables on a mesh that moves freely through the fixed cartesian grid. (Nematbakhsh et al., 2015) uses an immersed boundary method to investigate wave loads on a TLP wind turbine and compares with potential flow approximations. Showing good agreement at small wave heights. Alternatively, body fitted meshes can be used where the mesh is constructed around the structure, movement of the body is then achieved by morphing the shape of the mesh. To simulate floating responses specific boundary conditions can be applied on the body to induce mesh motion in accordance with hydrodynamic forces and the mass of the structure. For an example of a body fitted approach, (Chen et al., 2014) presents results for wave interaction with a vertical surface

piercing cylinder using OpenFoam's default two phase solver *InterFoam* which utilises a body fitted mesh and the VOF method of free-surface tracking with a new boundary for wave generation and absorption based on the work of (Morgan and Zang, 2011, Morgan et al., 2011) which reproduced experiments of the propagation of regular waves over a submerged bar, modelling up to the 8^{th} order harmonics correctly.

In terms of CFD application to WECs there are a few notable examples of Navier-Stokes type approaches being applied to model wave-structure interactions. (Yu and Li, 2011) performed a series of studies on a two-body heaving floating point absorber in operational wave conditions using RANS and VOF in StarCCM+. (Elhanafi, 2016)performed similar analysis on a 2D OWC and found that non-linear loading is more prevalent in vertical forcing than horizontal for his OWC case. (Agamloh et al., 2008) used the finite volume RANS code COMET (by CD-Adapco) to model the single degree of freedom dynamics of a heaving buoy WEC system in waves. COMET is a fluid-structure interaction model, employing VOF and has been used widely and validated. (Henry et al., 2013) compared characteristic wave impacts on an oscillating wave surge convertor calculated using two CFD approaches, namely a VOF method using OpenFOAM and a meshless particle method known as smoothed-particle hydrodynamics (SPH). Both VOF and SPH show 10% smaller amplitudes for flap motion compared to experiments. (Schmitt and Elsaesser, 2015) performed similar calculations using OpenFOAM's *InterDyMFoam* multiphase dynamic mesh solver and (Schmitt et al., 2012) highlights the problems faced when applying linearized potential flow codes such as WAMIT to the same case. (Iturrioz et al., 2015) provides a validation of OpenFOAM's *Interfoam* multiphase static mesh solver using wave generation and active absorption boundary conditions, based on the work of (Higuera et al., 2013), for simulation of a fixed detached 3D oscillating water column device, finding that "the model was proven to be able to reproduce the complex dynamics involved in an OWC device".

3 STRUCTURAL GEOMETRY AND COORDINATE SYSTEM

Figure 2 presents the WEC buoy 2D cross-section that is subject to hydrodynamic analysis in the presented project. Geometric details have been provided by Cruz Atcheson Consulting Engineers (www.cruzatcheson.com). The structure makes up a floating oscillating water column's (FOWC) cylindrical top-section that is positioned on the free-surface, thus experiencing a major share of the FOWC's total hydrodynamic loading, making it of significant interest for analysis. In the following work the buoy has been modelled as a closed structure in which the air chamber is not considered.

Full scale dimensions are given on the right-hand side of the figure and 1/20 scale model dimensions are shown on the left. A coordinate system definition is provided in which positive direction is indicated by each arrow's orientation.

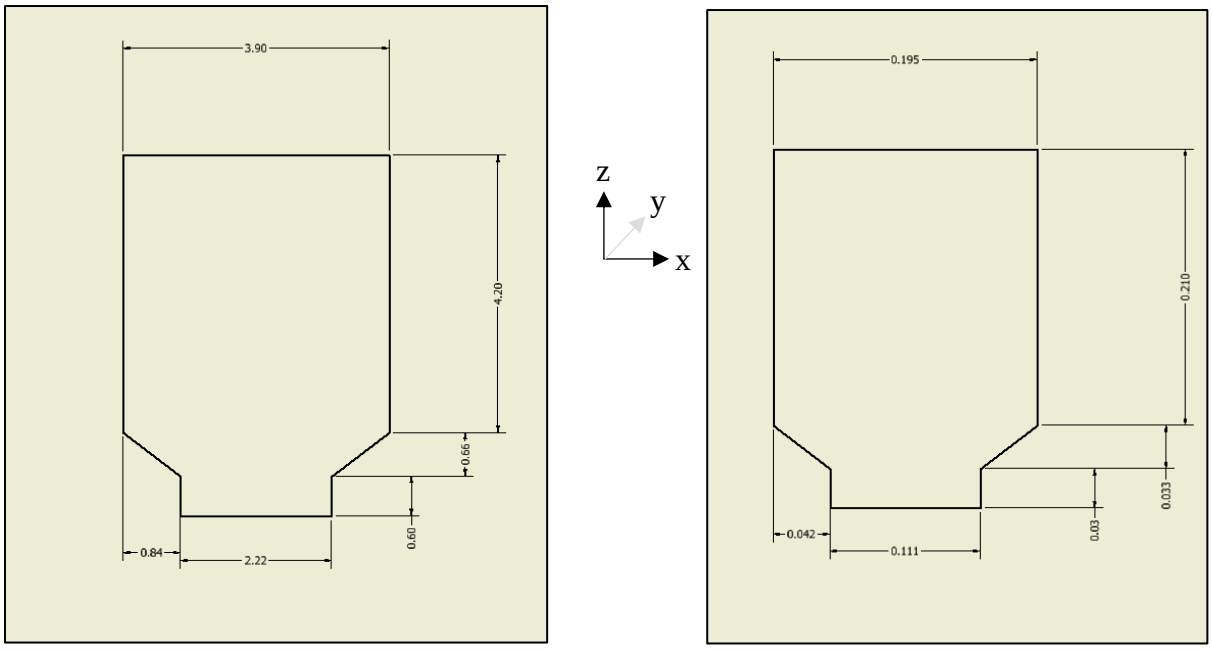

Figure 2. LHS: Full scale buoy geometry in metres, RHS: 1/20 model scale geometry in metres

The presented model scale dimensions are applied throughout the project in both numerical simulations and experimental tests. During analysis, the model is position on the free-surface with a draught of 0.189m.

It is useful at this point to define the buoy's leading edge, which is to be used for reference in the following sections. The term refers to the buoy's vertical left side spanning 0.21m. During analysis, the leading edge is tangential to the mean free-surface and exposed to incident waves propagating in the positive x direction.

4 EXPERIMENTAL METHOD

The presented laboratory test, completed in NTNU's Lader Tanken wave flume, is used to analyse the validity of wave induced heave forces calculated during numerical analysis. A high level of accuracy in experimental results is therefore fundamental for effective validation. The following section outlines the experimental method employed to obtain the vertical forces induced on a 1/20 scale model of the WEC buoy cross-section by waves of varying period and steepness. Both forces and wave elevation are measured to allow for comparison between experimental fluid dynamics (EFD) and CFD for the given problem.

It must be noted that the Lader Tanken facility is maintained by SINTEF Ocean, who have assisted in the experimental set-up and operation.

4.1 SET UP AND STRATEGY

4.1.1 Model specifications, tank parameters and instrumentation

A 3D representation of the 1/20 scale buoy cross-section has been constructed by SINTEF Ocean as a 59cm extrusion of the cross section in the y axis. Model dimensions, in millimetres, are provided in figure 3.

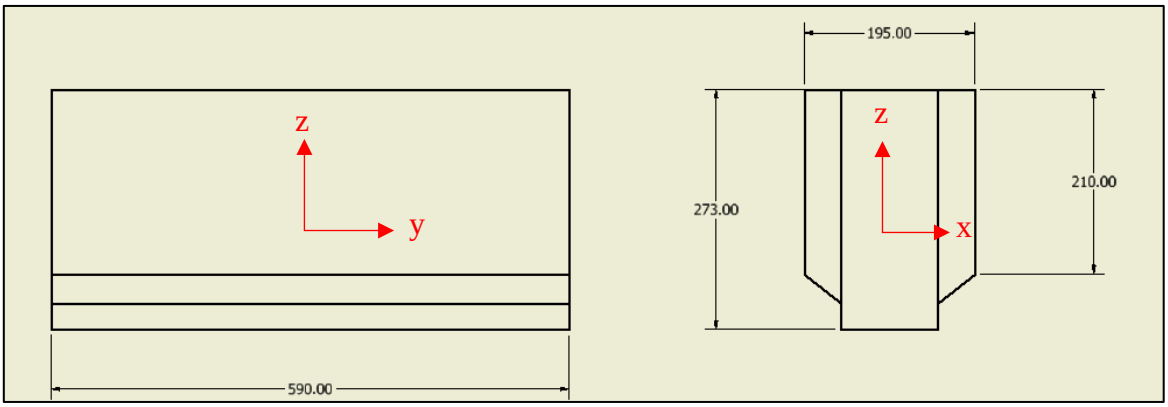

Figure 3. Model dimensions in mm

The model is fastened, at a distance from the wave maker paddle in its upright position to the leading edge of 6.4m in x, using a custom-made rig ensuring no lateral, vertical or rotational movement, as shown in figure 4. A zero-heel angle and a draught of 189mm is imposed.

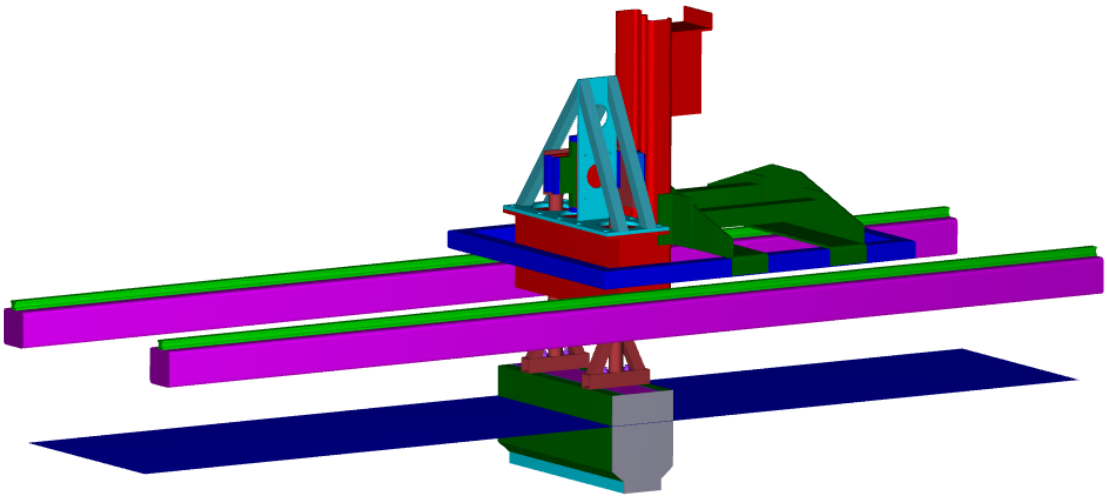

Figure 4. Experimental rig

Lader Tanken measures 13m in length, 0.6m in width and has been filled to a water depth of 1m. A wave dissipation beach is set up 5m behind the rear edge of the model to eliminate interference from waves reflected off the back end of the tank.

Vertical forces induced on the model are measured by a force transducer that connects the model to the rig. The transducer consists of strain gauges arranged in a Wheatstone bridge configuration. When the force is applied to the system, one strain gauge will be elongated on one side of the rod while the other is compressed on the other side, this introduces unbalance resistance in the bridge and voltage can be measured at the exit. A sampling frequency of 200 per second is used.

Positioning of the vertical force transducer is presented in figure 5.

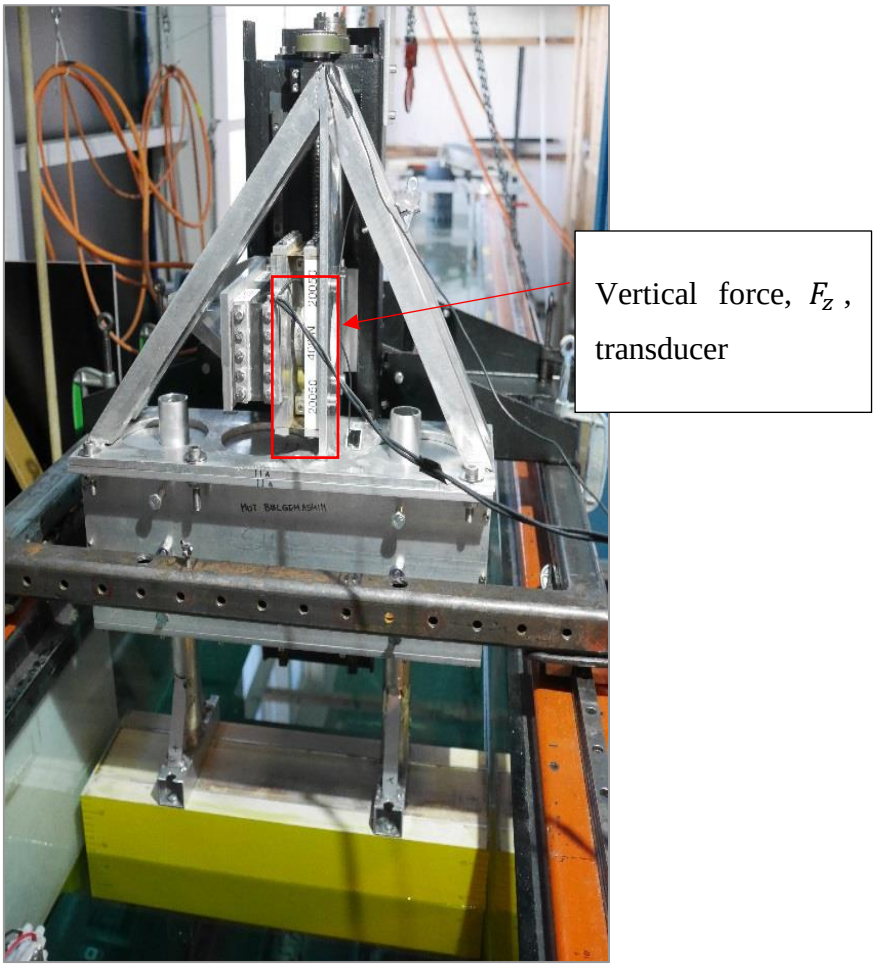

Figure 5. Vertical force transducer

Three wave probes are positioned in the tank observing wave elevation close to the model and to the wave maker, as detailed in table 1.

Table 1. Wave probe positions

Wave probe	**Distance from leading edge in x-direction, [m]**	**Distance from tank centreline in y-direction, [m]**
wp1	-0,50	-0,10
wp2	-0,50	0,10
wp3	-4,00	0,00

Wave probes one and two are depicted in figure 6.

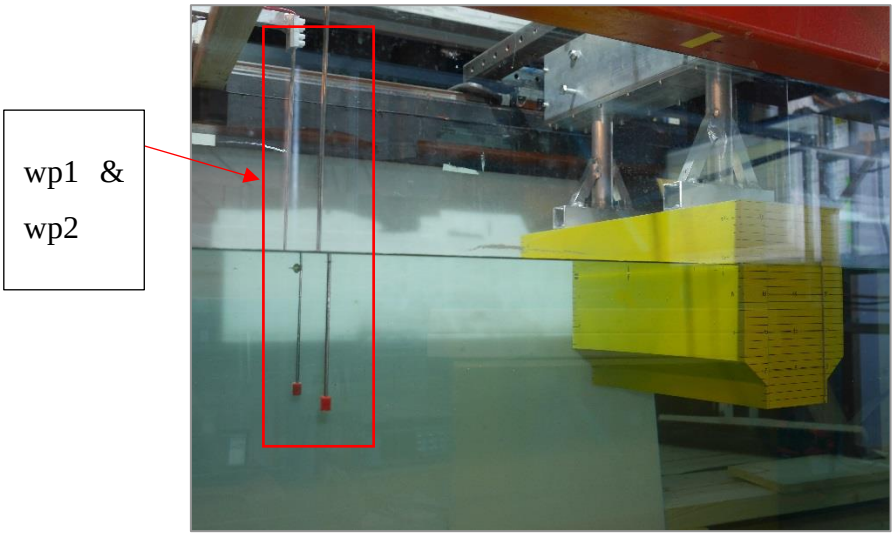

Figure 6. Wave probes at -0.5m

It is required that variation of wave effects is negligible across the tank in the y direction so that experimental results may be compared with the 2D numerical simulations after scaling. Wp1 and wp2 are used to test this assumption.

The wave maker consists of a single flap hinged at 120mm above the tank bottom and produces regular waves that propagate in the positive x-direction. A generation program, coded in MATLAB, is used to produce the required input data for the wavemaker. It is useful at this point to introduce some of the fundamentals on which the wave generation script is based.

4.1.1.1 Wave maker theory

(Dean and Dalrymple, 1991) reasons that wave motion induced by a wave maker and the power required may be determined from linear potential wave theory via solving a boundary value problem (BVP) in which an additional kinematic condition is satisfied on the wave maker at x equals zero. All other boundary conditions remain as in linear potential flow theory for marine applications, described in section 2.3.1**,** including a radiation condition far from the body in x.

A single flap wave-maker is utilised in the presented experiment which requires a specific boundary condition. After solving the BVP for velocity potential, φ, an expression is

determined for the wave elevation produced by the wave maker. The ratio between wave height produced and stroke of the flap, $^{H}/_{S}$, can be found, providing the key information required for operation. For a single flap in water depth *h*, hinged at a distance *hwm* below the free-surface at $z = 0$ the $^{H}/_{S}$ ratio for a wave with wave number *k* is defined by (Hughes, 1993) as,

$$^{H}/_{S} = \frac{4\sinh(\mathrm{kh})}{\sinh(2kh) + 2kh}\left[\sinh(kh) + \frac{\cosh(k(h - hwm)) - \cosh(kh)}{khwm}\right]$$

The wave generation script used in the presented experiments utilises this relation to set the flap motion to produce the desired wave heights. As stated by (Dean and Dalrymple, 1991), "wave maker theory has been developed assuming both small-amplitude motions of the paddle and small wave heights", thus for high steepness waves there is a level of unpredictability in the generated wave forms. A mechanical transfer function, developed from previous empirical experience, is therefore implemented to fine tune the flap motion such that it produces the desired wave heights for the specific tank and wave maker.

4.1.2 Calibration

Data acquisition sensors and transducers must be correctly calibrated i.e. the voltage induced in the sensors corresponds to the unit measured by means of an accurate calibration factor. The exact relationship between output signals and the known physical properties must therefore be found.

A generalized procedure for calibration is summarized below:

- A zero measurement is taken when the sensor is at its neutral position and is not disturbed by any environmental changes.

- Several different known values are set, the resulting voltages induced by the sensor are plotted graphically.

- The relationship between the known values and the voltage measured is given by the trend of several measurements. Calibration factor, $C\left[^{unit}/_{volt}\right]$, may then be obtained as the gradient of the line plot and logged in the data acquisition.

The vertical force transducer has a known calibration factor of 49.53 Newtons per volt measured, with a sensitivity equivalence of 3 millivolts per 1 volt. It is considered stable and has been used effectively in recent experiments, thus re-calibration was not carried out.

The wave probes have also been used effectively in recent experiments, however their calibration had to be checked. This was achieved by taking a zero measurement then raising the probes onto blocks of 49mm height. The measured change in height was within the allowable range of 49 +/- 1.5%, thus re-calibration was not required.

Calibration of the wave maker is achieved using the mechanical transfer function described previously. Due to the limited time frame of the experimental work, re calibration is not attempted, however wave making performance is assessed during analysis of wave elevation results.

4.1.3 Testing strategy and methodology

Four tests are carried out involving three wave periods. Each test consists of four runs with the same period but varying heights incorporating a steepness range from calm to storm conditions. Test details are provided by table 2, in which model and full-scale wave characteristics are provided.

Table 2. Tested wave characteristics

	Wave period, T [secs]	Full scale T [secs]	Wave steepness, H/λ	Wave number, k	Full scale k	Wave length, λ [m]	Full scale λ [m]	Wave height, H [m]	Full scale H [m]
Test 1 & 1a	0,80	3,58	1/60	6,288	0,314	0,999	20,010	0,017	0,333
			1/45	6,288	0,314	0,999	20,010	0,022	0,444
			1/30	6,288	0,314	0,999	20,010	0,033	0,666
			1/15	6,288	0,314	0,999	20,010	0,067	1,332
Test 2	1,00	4,47	1/60	4,027	0,202	1,560	31,182	0,026	0,520
			1/45	4,027	0,202	1,560	31,182	0,035	0,693
			1/30	4,027	0,202	1,560	31,182	0,052	1,040
			1/15	4,027	0,202	1,560	31,182	0,104	2,080
Test 3	1,20	5,37	1/60	2,815	0,141	2,232	44,688	0,037	0,744
			1/45	2,815	0,141	2,232	44,688	0,050	0,992
			1/30	2,815	0,141	2,232	44,688	0,074	1,488
			1/15	2,815	0,141	2,232	44,688	0,149	2,976

Tests 1 and 1a are identical, permitting experimental precision to be briefly examined in the following section.

Before each test, 30 second zero-setting measurements are taken such that constant environmental conditions are neglected, making results from all tests comparable.

Each run consists of 3 ramp-up, 19 regular and 3 ramp-down periods. Time has been given between runs allowing the tank to settle. 310 seconds has been utilised, yielding very small amounts of free-surface disturbance at the start of each run.

4.2 EXPERIMENTAL PRECISION, WAVE MAKER PERFORMANCE AND FREE SURFACE VARIATION IN Y

The following section utilises results from 0.8s period waves to investigate experimental precision as well as two additional factors, namely wave maker performance, affecting accuracy of the experimental forces, and free-surface variation in y which affects the ability to make comparisons between experimental results and numerical work.

Wave induced vertical force time series for tests 1 and 1a are presented in figure 7, providing an indication of experimental precision.

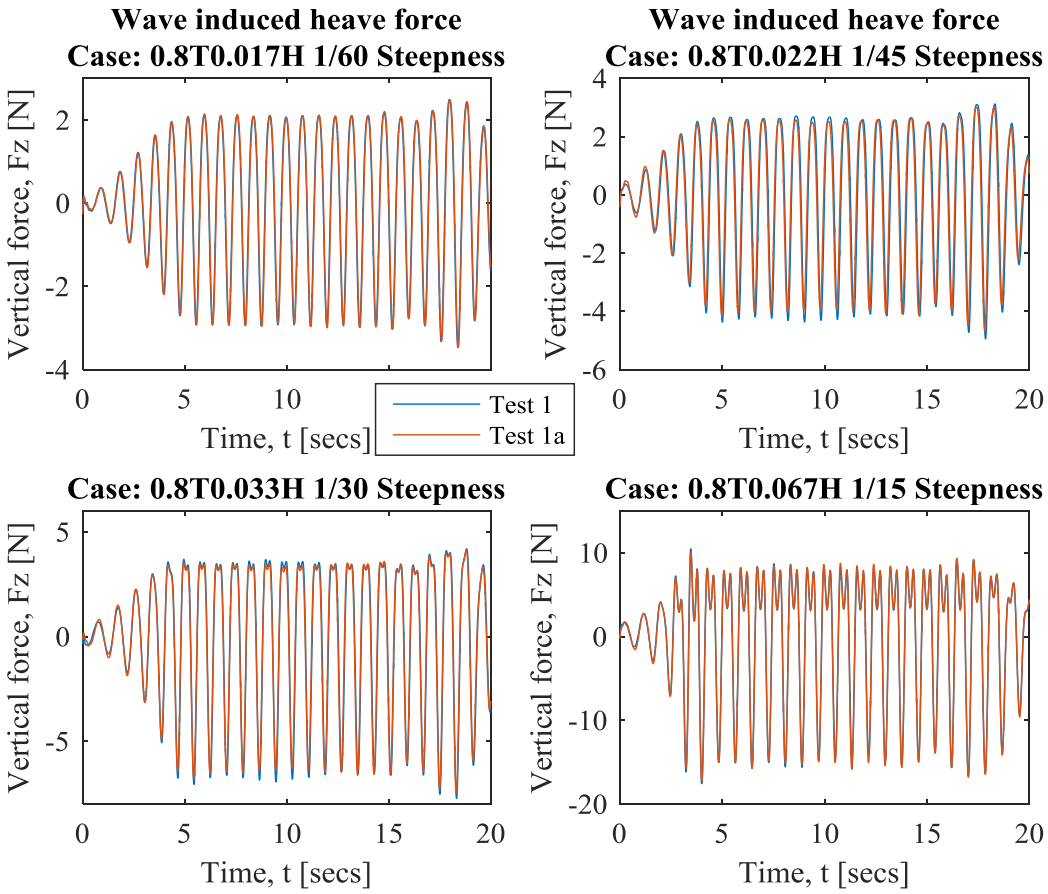

Figure 7. Test 1 & 1a wave induced heave forces

Very little discrepancy is seen between the results of the two tests. Time series variations are replicated almost exactly, indicating an appropriate level of experimental precision.

Wave elevation at wp3 is compared for tests 1 and 1a in figure 8. This serves to examine experimental precision as well as wave maker performance.

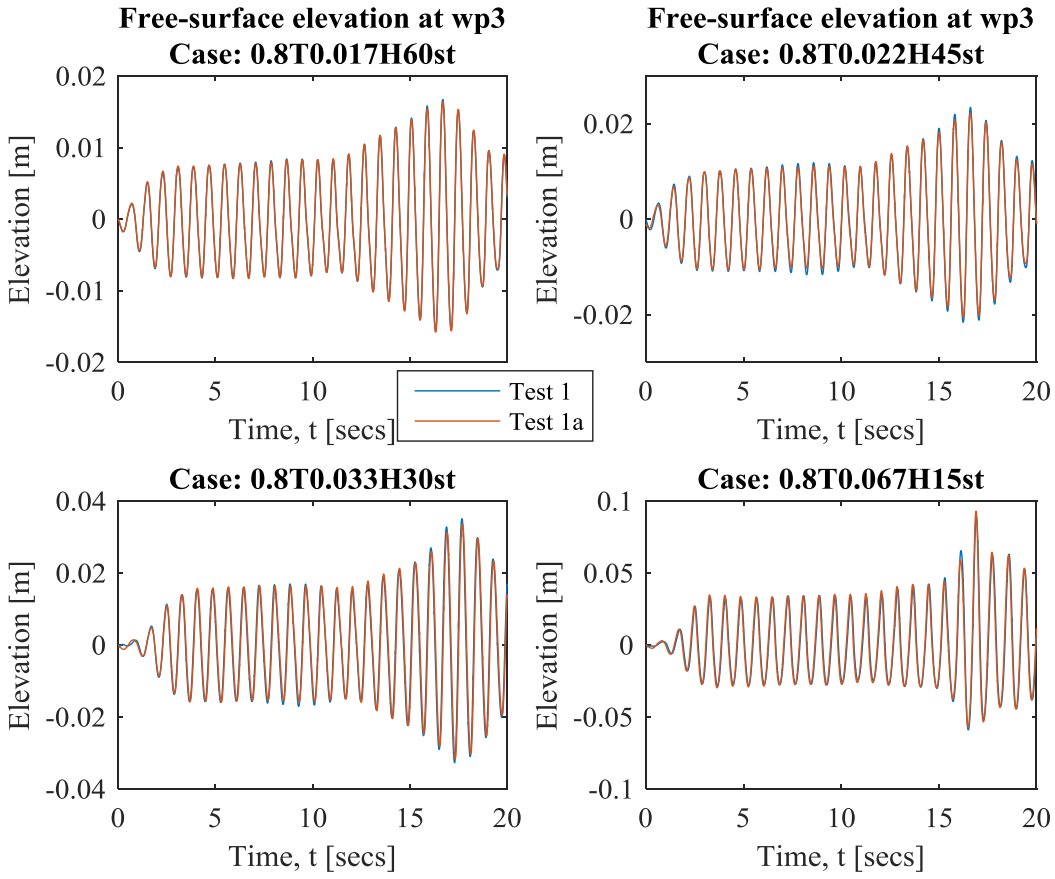

Figure 8. Test 1 & 1a free-surface elevation at -4m from leading edge

Again, good agreement is seen between the results of test 1 and 1a. Table 3 provides the average wave heights produced by the wave maker within steady state regions between 4 and 11 seconds, in which wave reflection from the body is yet to affect the free-surface elevation. For accurate wave induced forces, this measured average wave height should be as close as possible to the set theoretical heights: also included in table 3.

Table 3. Wave maker performance at 0.8 second T

Wave steepness, H/λ	Set wave height, H [m]	Average measured wave elevation [m]	
		Test 1	Test 1a
1/60	0,017	0,016	0,016
1/45	0,022	0,022	0,021
1/30	0,033	0,033	0,032
1/15	0,067	0,061	0,062

One observes close agreement between the measured values of test 1 and 2, hinting at good experimental precision. The measured values are also very close to the theoretical heights for the 1/60, 1/45 and 1/30. Wave making performance slightly reduces for the steeper 1/15 waves; with an average discrepancy between measured and theoretical heights of 8%.

It is also important to investigate the variation of wave elevation in the y-direction thus wp1 and wp2 data from test 1 are presented in figure 9.

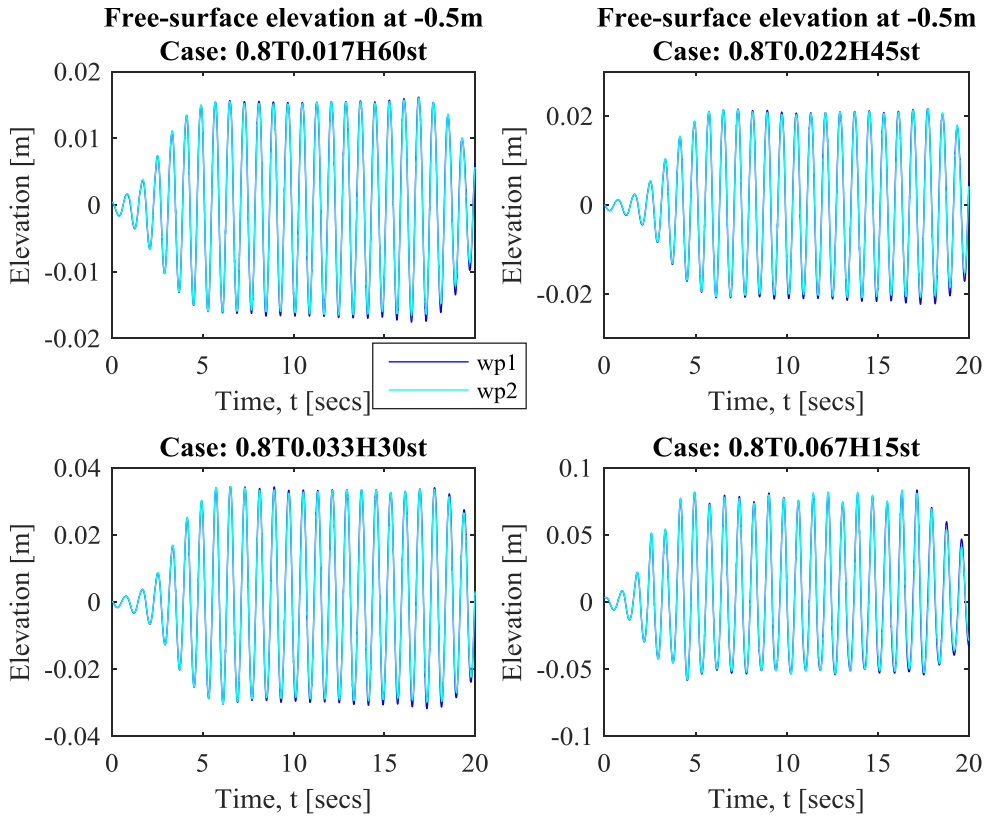

Figure 9. Free surface variation at -0.5m from leading edge

Differences are quantified in table 4 where average heights measured by wp1 and wp2 are compared for steady state regions between 6 and 15 seconds.

Table 4. Free-surface y-variation for test 1

Wave steepness, H/λ	Average measured wave elevation [m]	
	wp1	wp2
1/60	0,032	0,032
1/45	0,042	0,041
1/30	0,064	0,062
1/15	0,130	0,130

Negligible variation is seen at wp1 and wp2, positioned at -0.1 and 0.1m in y from the tank centre line respectively, thus it is assumed that wave elevation is constant in y during test 1. This helps to confirm that scaled experimental results are comparable to the those produced by 2D numerical simulations.

5 NUMERICAL METHOD

Fixed and floating case CFD simulations are carried out by means of parallel computation on four Intel® Xeon® CPU E5-2630 v3 @2.40GHz cores using the open source software OpenFOAM® v1612+: developed and released by OpenCFD Ltd. OpenFOAM employs the finite volume method (FVM) for modelling viscous fluid flows, for details on the fundamentals of this approach the reader should refer to section 2.3.2 in chapter 2.

For all the presented numerical work, air and water phases are defined as Newtonian fluids with kinematic viscosities of $1.48\times10^{-5}$and $1\times10^{-6}\ m^2/s$ and densities of 1 and 1000 kg/m^2 respectively.

Turbulence modelling is not performed as turbulent effects are assumed to be insignificant for the given cases. The main effect of turbulence is the variation of flow separation point positions on the body, this is of concern for curved structures such as cylinders. For sharp cornered structures such as the geometry in question, separation points are always at corners. Excluding turbulence models results in laminar computations, in which direct Navier Stokes solutions are found at low resolution. Details are not modelled down to Kolmogorov scale as in DNS type CFD but the approach is identical.

5.1 FIXED CASE SIMULATIONS

Replication of the experimental work using OpenFOAM is undertaken. Simulation of regular gravity waves incident to a fixed structure requires a static two-phase solver. For this, OpenFOAM's default multiphase solver, *InterFoam*, is employed, in a similar fashion to (Chen et al., 2014), (Iturrioz et al., 2015) and (Diz-Lois Palomares, 2015).

Twelve wave forms are simulated, reproducing tests 1, 2 and 3 of the experiments. To recap, test 1 uses 0.8s period waves, test 2 uses 1.0s and test 3 uses 1.2s. Every test includes runs of wave steepness 1/60, 1/45, 1/30 and 1/15. The total time of each numerical run is calculated as 30 times the wave period. Forces induced on the body are computed through pressure integration using OpenFOAM's *forces* function object in which density of the fluid has been set at $1000\,kg/m^3$. For simulation control an adjustable time step is utilised, determined by a maximum allowable Courant number of 0.65.

5.1.1 Numerical schemes and solution algorithms

InterFoam is designed for unsteady, incompressible multiphase problems and utilises the VOF free-surface tracking technique. The solver adopts the PISO algorithm, in which pressure is linked to velocity using a modified Poisson equation, representing mass continuity within the system and the 1st NS governing equation. Two separate pressure and velocity corrections are made per iteration of the PISO algorithm loop.

Appropriate numerical schemes must be chosen for the discretization of the NS momentum equation plus the transport equation for the fluid phase fraction, α. Time discretization schemes, *ddtSchemes*, are required for the temporal terms. Divergence schemes, *divSchemes*, are required for the convective terms. Gradient and Laplacian schemes, *gradSchemes* and *laplacianSchemes*, are needed to model the diffusive terms. Interpolation schemes, *interpolationSchemes* specify how transported property values at cell faces are evaluated and finally for discretization of surface normal gradients, *snGradSchemes*, are required.

In the presented project, all numerical schemes except for *divSchemes* and *ddtSchemes* are kept as the defaults provided in *InterFoam* wave based tutorials. Defaults include second

order *gradSchemes, laplacianSchemes, interpolationSchemes* and *snGradSchemes*. A further explanation of the choices available for OpenFOAM's *divSchemes* is given below.

For convective fluxes, i.e. *divSchemes,* a first order scheme exists called the upwind method, this is very stable and outputs bounded (non-oscillatory) solutions, however it is inaccurate due to high levels of numerical diffusion. Linear or central differencing is second order accurate but generates oscillatory solutions. The linear upwind method is also second order accurate but more stable, only becoming unbounded in highly convective flows where there are strong gradients. Total variation diminishing (TVD) methods, such as VanLeer and SuperBee apply slope limiters to the linear upwind method that switches the method to the first order upwind method when strong gradients are detected, helping to prevent oscillatory solutions. For initial simulations, the linear upwind method is selected for the convective terms in the NS momentum equation and the TVD VanLeer method is used for convective terms in the phase fraction transport equations.

When using the solver *InterFoam* for transient simulations, two choices are available for discretization of the temporal term, i.e. *ddtSchemes.* There is the first-order accurate implicit Euler method which has been utilised in the presented project and the second-order implicit Crank Nicolson method. Both produce bounded solutions. Theoretically Crank Nicolson should produce more accurate solutions but can be very unstable and requires an off-centring coefficient which blends the two methods together. It should also be noted that some important features of the *InterFoam*'s VOF implementation are not possible when using Crank Nicolson such as sub-cycling: a form of temporal filter to improve stability. For initial simulations Euler's method is selected for temporal discretization.

With the transport equations appropriately discretized and applied to each control volume, they must be organised into large matrices describing the whole domain to which boundary conditions are numerically implemented, enforcing the physical characteristics of the simulation. To solve the linear systems of equations a range of algorithms exist. For the presented simulations a generalised geometric-algebraic multi-grid method, *GAMG,* has been selected for the symmetric pressure matrices. The preconditioned biconjugate gradient solver, *PBiCG,* is chosen for the asymmetric velocity matrices. A custom solver incorporating Gauss Seidel's iterative method for linear systems is utilised for the α matrices.

5.1.2 Computational domain and boundary conditions

A body fitted mesh approach is applied to model the 1/20 scale buoy geometry within a computational domain. The buoy structure has been developed in Autodesk Inventor CAD software and exported as an STL file. OpenFOAM's built-in complex meshing tool, *snappyHexMesh*, is used to construct a mesh around the input geometry file. *snappyHexMesh* generates 3D meshes by splitting a background mesh, containing cells with aspect ratio 1, around the geometry. Cells within the body are removed and those along structural edges are distorted to snap onto the body. As the presented project involves 2D simulations, an extrusion is taken of the domain's centreline plane with a thickness of 0.01m in the y direction. One cell is used for this extrusion, as is the general approach for 2D modelling in OpenFOAM.

The domain is created with an initial span of 10m in x and boundaries are assigned as in figure 10. The WEC buoy-section is positioned on the free-surface with a draught of 0.189m in a water depth of 1m, thus replicating the experimental wave flume set-up.

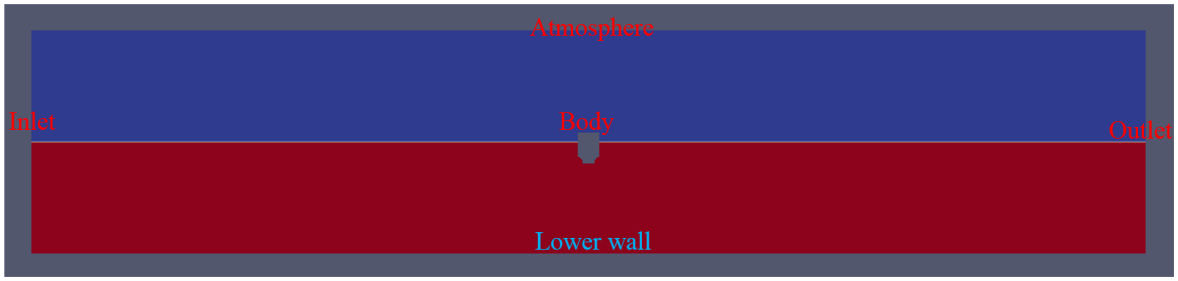

Figure 10. Numerical domain and boundaries

Initial mesh refinement is applied along the free-surface and around the body, as displayed in figures 11 & 12.

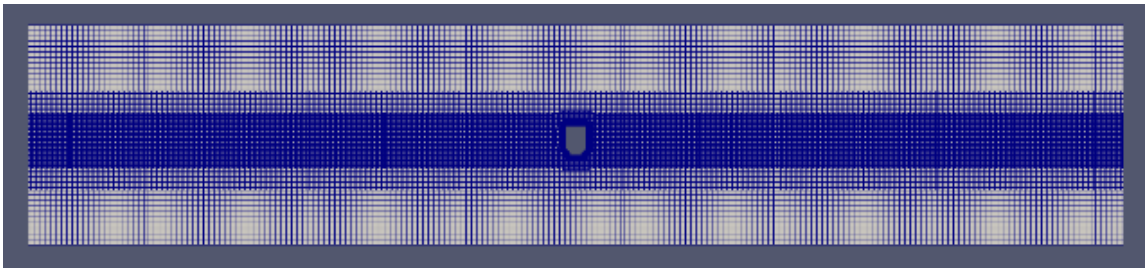

Figure 11. Mesh refinement along free surface region

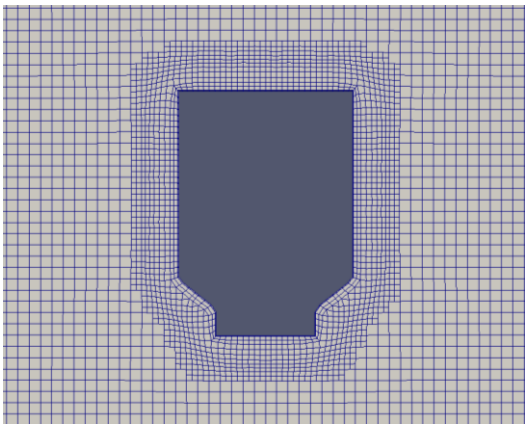

Figure 12. Mesh refinement around body

Table 5 provides the boundary conditions applied to the computational domain plus their initial values at $t = 0$. The internal cells must also be assigned initial values. For pressure and velocity zero values are set throughout the domain. Phase fraction values are applied using the *setFields* utility to define the initial free surface position, with values of one below and zero above.

Table 5. Fixed case boundary conditions

Boundary field	**Boundary type**	**Velocity, U**	**Pressure, P**	**Phase fraction, α**
		BC	**BC**	**BC**
Body	Wall	*fixedValue uniform (0 0 0)*	*zeroGradient*	*zeroGradient*
Inlet	Patch	*waveVelocity uniform (0 0 0)*	*fixedFluxPressure uniform (0)*	*waveAlpha uniform (0)*
Outlet	Patch	*waveVelocity uniform (0 0 0)*	*fixedFluxPressure uniform (0)*	*zeroGradient*
Lower wall	Wall	*fixedValue uniform (0 0 0)*	*fixedFluxPressure uniform (0)*	*zeroGradient*
Atmosphere	Patch	*pressureInletO-utletVelocity uniform (0 0 0)*	*totalPressure uniform (0)*	*inletOutlet uniform (0)*
Front and Back	Empty	*empty*	*empty*	*empty*

Empty conditions are used for patches whose plane is normal to the y direction and require no solution in 2D simulations. A no slip condition on the lower wall and body, consistent with viscous flow theory, are enforced. Wave generation and active absorption is

achieved through the *waveVelocity* and *waveAlpha* BCs: developed at the Environmental Hydraulics Institute, IHCantabria and described in (Higuera et al., 2013). Velocity is prescribed corresponding various wave theories. The appropriate theory must be selected in accordance with figure 1: taken from (Le Mehaute, 2013). Only Stokes's wave theories, up to 5^{th} order, are used in the presented simulations. Examples involving successful implementation of these wave generation and absorption BCs are given in (Iturrioz et al., 2015) and (Diz-Lois Palomares, 2015).

5.1.3 Sensitivity studies

With the initial set-up defined it is important to investigate the sensitivity of certain parameters fundamental to accurate CFD simulations, namely the mesh characteristics, domain span as well as the choice of convective and temporal discretization schemes. Multiple simulations of the 0.8 second period wave with 1/60 steepness are performed, in which these parameters are varied. It is envisaged that results from the presented studies are representative across the test range however this has not been verified due to time restrictions on the project.

5.1.3.1 Mesh study

Six meshes have been constructed using *snappyHexMesh* with a background mesh made up of $0.05m \times 0.05m$ square cells. Different levels of refinement are applied to the free-surface and body region for each mesh. A level 1 refinement of a background mesh cell involves halving the height and width, thus 4 refined cells take up the space of one original cell. Table 6 gives the mesh characteristics tested for the 0.8T0.017H 1/60 steepness case.

Table 6. Mesh characteristics

Mesh	Refinement along FS	# cells per H	# cells per λ	Refinement around body	# cells over leading edge
1	Level 1	0,68	39,97	Level 2	17
2	Level 2	1,36	79,94	Level 2	17
3	Level 2	1,36	79,94	Level 3	34

4	Level 3	2,72	159,87	Level 3	34
5	Level 3	2,72	159,87	Level 4	68
6	Level 4	5,44	319,74	Level 4	68

Figure 13 below presents the vertical wave induced forces measured on the structure during simulations with the six alternative meshes. By-pass filtering is applied to the force data, removing high frequency noise as well as mean loads, so that experimental and numerical results may be easily compared. This is necessary as the *forces* function object has been used to compute total force whereas hydrostatic pressure force was removed from experimental data during zero-setting procedures. This filtering involves fast Fourier transforms of the force time series, cut-off frequencies are then applied before the filtered frequency spectrum is subjected to an inverse Fourier transform, resulting in a filtered time series. Cut off frequencies are taken as 0.1 and 4 times the wave frequency, retaining those in between.

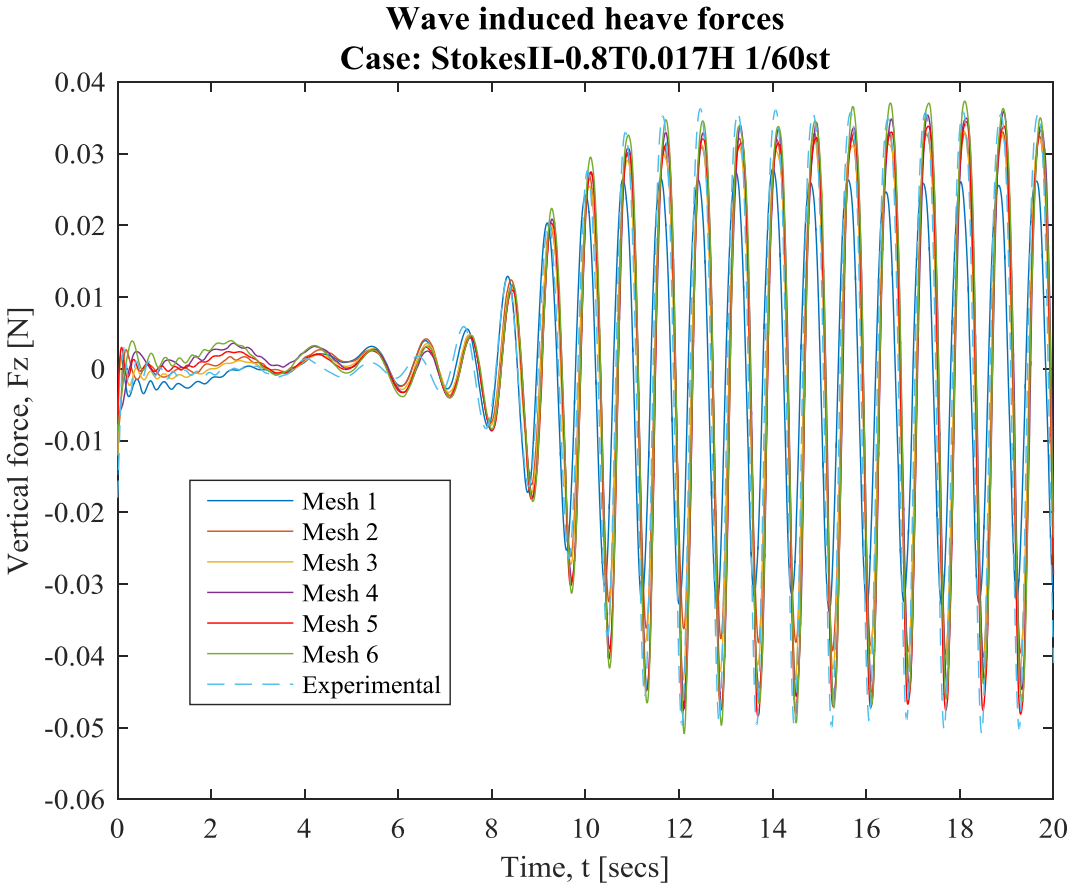

Figure 13. Mesh study- Heave forces

Taking the average heights within the steady state region of 12 to 19 seconds and comparing them with the experimental value in table 7 helps to quantify differences between meshes.

Table 7. Mesh study- Average force values

	Experimental	**Mesh 1**	**Mesh 2**	**Mesh 3**	**Mesh 4**	**Mesh 5**	**Mesh 6**
Average force oscillation height [N]	0,0854	0,0587	0,0714	0,0736	0,0794	0,0804	0,0824

One sees significant improvement in the mesh's ability to reproduce the experimental measurement for those with refinement of level 3 and above on the body and free-surface, i.e. meshes 4, 5 and 6, all of which produce average heights with a discrepancy of less than 10% of the experimental result. This is a good indication that the numerical results have a level of validity. Mesh 4 yields a force value within 7% of the measured experimental result, mesh 5 gives 6% and mesh 6 is clearly the most effective with a discrepancy of only 4%, however additional factors must be considered before final selection.

It is of interest to examine the wave modelling capabilities of each mesh. As in the experimental procedure, wave elevation is probed at -0.5m and -4m in x from the leading edge of the model. Figure 14 presents wave elevation at -4m which corresponds to wp3 in the experimental tank, thus results are compared with experimental data.

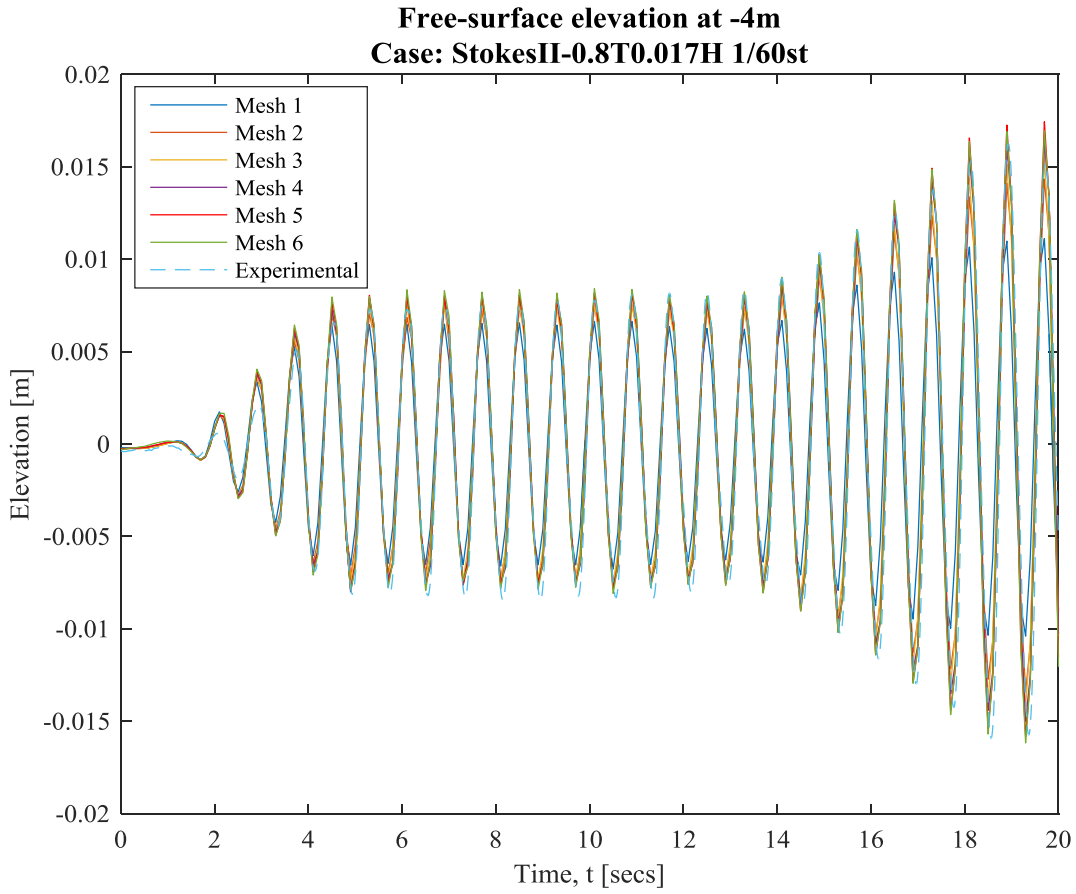

Figure 14. Mesh study- Wave elevation at -4m

Average wave heights within the steady state region of 5-12s are taken and presented in table 8. The theoretical wave height is provided for reference, as in the steady region wave reflection from the model is yet to take effect and thus accurate elevation data should compare well.

Table 8. Mesh study- Average wave heights

	Theoretical	**Experimental**	**Mesh 1**	**Mesh 2**	**Mesh 3**	**Mesh 4**	**Mesh 5**	**Mesh 6**
Average wave height [m]	0,0167	0,0159	0,0131	0,0147	0,0149	0,0155	0,0157	0,0160

Again, we see good agreement between the experimental measurement and the numerical results. Less than 10% discrepancy is seen for meshes 2-6. Meshes 4, 5 and 6 are however superior and produce results within 10% of the theoretical value, with mesh 6 actually outperforming the wave makers ability to reproduce the set wave characteristics

during wave flume experiments. The meshes ability to reproduce the desired wave elevation seems to be consistent with its ability to replicate experimental forces.

A mesh must be chosen such that it induces as little numerical damping of the waves as possible. Wave elevation is sampled during each simulation within the mesh study at -4m, -3m and -2m. The difference between steady state solutions at these points is obtained and an average of the two values is taken to find a value for numerical wave damping per metre. Table 9 displays such values as percentages of the theoretical wave height.

Table 9. Mesh study- Wave damping

	Mesh 1	**Mesh 2**	**Mesh 3**	**Mesh 4**	**Mesh 5**	**Mesh 6**
Average numerical damping of waves per meter [% theoretical height]	7,78	6,23	3,51	2,63	2,16	2,18

Convergence in numerical damping results occurs for meshes 5 and 6, meaning that there is no advantage gained using mesh 6. Only a small improvement is seen between meshes 4 and 5.

It is also crucial to consider the run times for each simulation, presented in table 10, as this influences the usability of the mesh.

Table 10. Mesh study- Run times

Mesh	**Run time**		
	[hours]	**[mins]**	**[secs]**
1	0	4	48
2	0	16	11
3	0	19	34
4	2	29	12
5	3	4	26
6	21	8	40

On completion of the presented mesh study it is clear that increasing the level of mesh refinement on the body and along the free-surface is beneficial for improving force and wave elevation accuracy, as well as reducing wave damping. For the 0.8T0.017H case significant improvements in the meshes ability are seen when using refinement level 3, compared to coarser mesh results. Tables 7, 8 and 9 suggest that only modest improvements can be gained using meshes with finer meshes. The time cost required for such improvements is too expensive due to the time restrictions on the project. Mesh 4, with refinement level 3 on the body and free-surface, has thus been selected for the presented fixed body simulations.

It should be noted that the selected mesh refinement at the inlet boundary was not suitable for waves of steepness greater than 1/30, as air pockets formed due to reflected waves causing simulations to crash. For such cases courser meshes have been applied close to the inlet. All other mesh characteristics have been kept constant across all fixed case tests.

5.1.3.2 Domain study

With mesh refinement selected it is of interest to observe the effect of domain size on simulation results. In this way, one can determine whether the full experimental tank must be modelled numerically.

The experimental model was positioned at a -6.4m from its leading edge to the wavemaker. Vertical force results are compared for two simulations, one full-length domain spanning -6.4m from the leading edge and one with a shortened domain spanning -5m from the leading edge. Forces have been band pass filtered between 0.1 and 4 times the wave frequency, removing high frequency noise and mean loads such that experimental and numerical results are comparable.

Average force oscillation heights of the respective steady state regions are given in table 11.

Table 11. Domain study- Average force values

	Experimental	**Whole-Tank**	**Short-Tank**
Average force oscillation height [N]	0,0856	0,0703	0,0737

There is no improvement in force results when modelling the whole tank in front of the structure therefore computational costs may be saved using the shortened domain.

5.1.3.3 Numerical study

A brief investigation has been carried out in which the effect of changing convective and temporal schemes is examined.

For *divSchemes,* using the linear method rather than the linear upwind for the convection terms in the momentum equation method introduced instability and simulations crashed after a short time. Using SuperBee for convection in α produced average wave elevation and force results with a discrepancy of less than 1.1% when compared to VanLeer and required a very similar run time. No noticeable improvements were observed whilst testing the sensitivity of convective discretisation schemes thus the initial numerical set up using the linear upwind and VanLeer methods is maintained throughout the project.

For *ddtSchemes,* the effectiveness of the second order implicit Crank Nicolson method is compared with Euler's first order method. Using purely Crank Nicolson is unstable, causing immediate crashes, thus an off-centring parameter of 0.9 has been set. Improvement is seen using Crank Nicolsen when observing wave elevation, presented in figure 15.

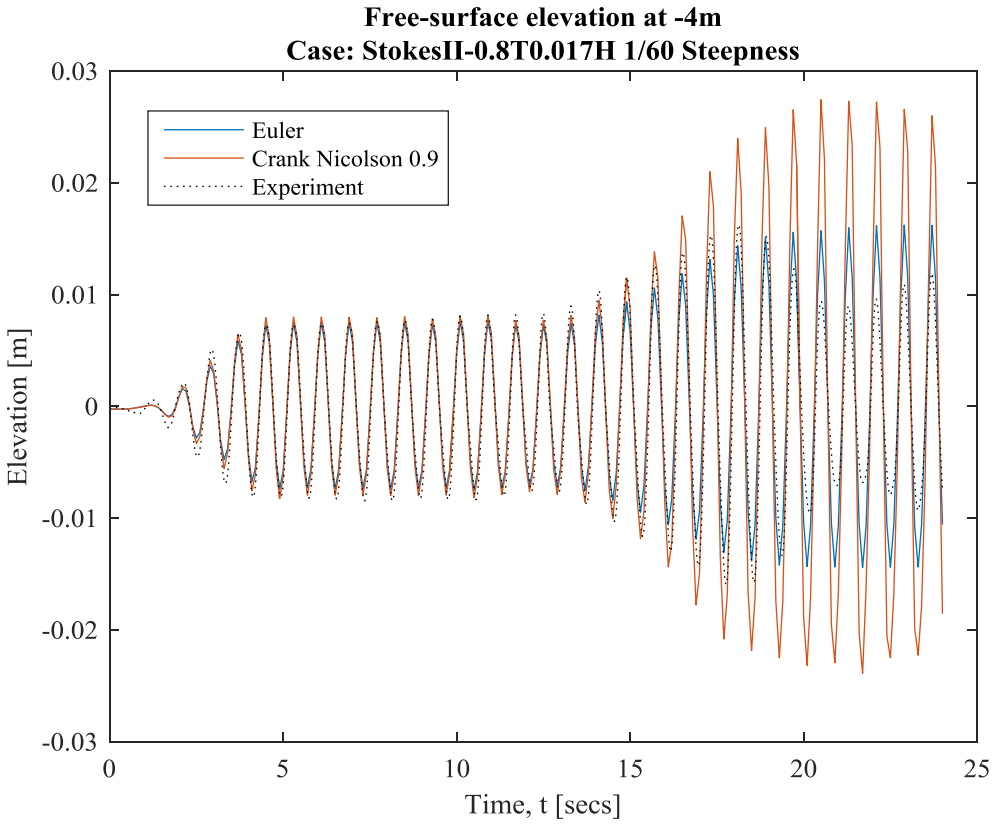

Figure 15. Time discretisation study- Wave elevation at -4m

The Crank Nicolson method provides a 7% improvement, measured as difference over initial Euler value, in replicating the experimental values within the 5-12 second region. However, when observing measured forces, the Crank Nicolson method drastically overshoot the experimental data, as shown in figure 16.

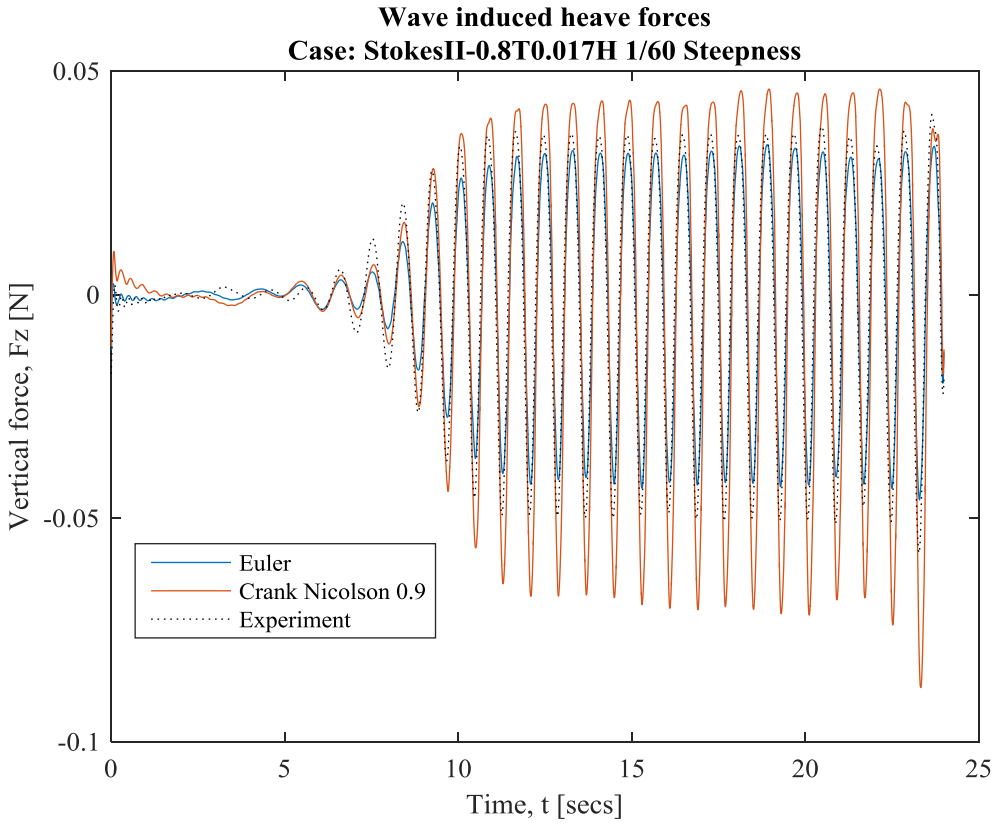

Figure 16. Time discretisation study- Heave forces

The initial set up using Euler's method is maintained for further numerical work.

5.2 LINEAR FORCES

To numerically compute excitation forces based on linear potential flow theory, a boundary element method (BEM), as described in section 2.3.1, would generally be used. However commercial linear potential flow software such as WAMIT does not have the capacity to make 2D calculations or replicate the wave flume test conditions. Due to time restrictions on the presented project, constructing a potential flow code for the buoy section geometry was not practical. Instead OpenFoam has been used to simulate very small steepness waves and calculate the pressure forces on the body. Wave steepness has been chosen in accordance with (Le Méhauté, 1969) and implementing a water depth of 1 metre, such that the wave is known to be described accurately by linear potential flow theory. If the set amplitude is small relative to the body such that the free surface remains along the straight side edge of the buoy then non-linear inertial effects as well as viscous effects are likely to be negligible and thus OpenFoam is imitating linear potential flow calculations. This method renders obsolete the error experienced in linear potential pressures under wave troughs.

Waves with steepness 1/200 over a period range of 0.75 to 1.5 seconds fall within linear theory's range of applicability. Twelve such wave forms have been simulated using *InterFoam* and vertical forces induced on the body are measured. Characteristics are provided in table 12.

Table 12. Linear wave characteristics

Wave period, T [s]	Wave number, k	Wave length, λ [m]	Wave height, H [m]	1/Steepness, λ/H	kA
0,75	7,154	0,878	0,004	200	0,0157
0,80	6,288	0,999	0,005	200	0,0157
0,85	5,570	1,128	0,006	200	0,0157
0,90	4,969	1,265	0,006	200	0,0157
0,95	4,460	1,409	0,007	200	0,0157
1,00	4,027	1,560	0,008	200	0,0157
1,05	3,655	1,719	0,009	200	0,0157
1,10	3,334	1,884	0,009	200	0,0157
1,15	3,057	2,056	0,010	200	0,0157
1,20	2,815	2,232	0,011	200	0,0157
1,25	2,604	2,413	0,012	200	0,0157
1,50	1,875	3,351	0,017	200	0,0157

For comparison with the fixed case CFD calculations described in section 5.1, the linear forces for 0.8, 1.0 and 1.2s periods are scaled to the appropriate wave heights. This is valid under linear theory as forces are assumed to be proportional to wave height.

5.3 FLOATING CASE SIMULATIONS

The numerical work goes on further to investigate heave response of the WEC buoy-section. Floating simulations are carried out for the same wave periods and steepness as in the fixed tests 1, 2 and 3.

OpenFOAM's dynamic VOF solver *InterDyMFoam* is utilised. This is similar to the fixed case solver, *InterFoam* but incorporates mesh deformations to model motion. An additional set of equations must therefore be solved describing the displacement of cell nodes within the mesh, known as point displacements. A pre-conjugate gradient matrix algorithm is used for the extra system of equations.

Specific boundary conditions are required to model point displacements within the domain and fluid velocities on a moving wall. Mesh deformation is based on the pressures exerted on dynamic boundaries and is computed using the *displacementLaplacian* solver. Table 13 provides the BCs for the floating case simulations, with their initial values.

Table 13. Floating case boundary conditions

Boundary field	**Boundary type**	**Velocity, U**	**Pressure, P**	**Phase fraction, α**	**Point displacement**
		BC	**BC**	**BC**	**BC**
Body	Wall	*movingWallVelocity uniform (0 0 0)*	*zeroGradient*	*zeroGradient*	*sixDOFRigidBodyDisplacement*
Inlet	Patch	*waveVelocity uniform (0 0 0)*	*fixedFluxPressure uniform (0)*	*waveAlpha uniform (0)*	*fixedValue uniform (0 0 0)*
Outlet	Patch	*waveVelocity uniform (0 0 0)*	*fixedFluxPressure uniform (0)*	*zeroGradient*	*fixedValue uniform (0 0 0)*
Lower wall	Wall	*fixedValue uniform (0 0 0)*	*fixedFluxPressure uniform (0)*	*zeroGradient*	*fixedValue uniform (0 0 0)*
Atmosphere	Patch	*pressureInletOutletVelocity uniform (0 0 0)*	*totalPressure uniform (0)*	*inletOutlet uniform (0)*	*fixedValue uniform (0 0 0)*
Front and Back	Empty	*empty*	*empty*	*empty*	*empty*

The *sixDOFRigidBodyDisplacement* BC requires some explanation here. Using pressure integration to calculate forces on the body boundary motion is calculated in accordance with Newton's second law of motion. For this, the body's mass and centre of mass coordinates must be provided. In the presented work mass has been calculated as the volume of displaced fluid multiplied with the fluid density of 1000 kg/m^3, giving 0.3272 kg. The

aim of the floating simulations is to investigate heave motion of the buoy, measured using the centre of mass for reference. To achieve this, constraints are applied within the boundary condition such that motion is restricted to a single degree of freedom in z. Due to body symmetry, pitch (rotation around the y axis) does not need to be considered as it has no influence on the heave response at the centre of mass.

Any simulation parameters that are not specified above, including boundary conditions, mesh characteristics, domain size, numerical schemes and solution algorithms, are kept constant as in the fixed case computations. Once again, the *forces* function objective is utilised and response of the centre of mass is extracted from each simulation's logged data.

5.4 LINEAR RESPONSE

A linear response simulator is developed in MATLAB. Responses to linear wave forces are computed by solving the following equation of motion.

$$(m + A_{33})\ddot{\eta}_3 + B_{33}\dot{\eta}_3 + C_{33}\eta_3 = F_{exc}$$

Linear excitation forces which include Froude-Krylov and diffraction forces, are calculated for the wave period range 0.75 to 1.5 seconds, as described in section 5.2. The linear hydrodynamic forces exerted on the body by the fluid are found from forced oscillations with frequency equal to that of the waves. This procedure is outlined in the following section.

MatLab's inbuilt ODE45 function is used to solve the above second order ordinary differential equation for each linear excitation force, F_{Exc}, outputting heave displacement time series. Hydrodynamic coefficients are kept constant for each excitation wave, thus the equation is solved in the frequency domain, mimicking software such as WAMIT.

5.4.1 Linear hydrodynamic coefficients

Once again OpenFOAM has been used to imitate linear potential flow calculations. Hydrodynamic forces on a body are computed by solving radiation problems in which forced oscillations are applied to the body. Small heave oscillations are enforced using *InterDyMFoam*. The numerical set-up remains the same as for the floating case CFD

simulations apart from one alternation in the point displacement boundary conditions, as shown in table 14.

Table 14. Floating case boundary conditions

Boundary field	**Boundary type**	**Velocity, U**	**Pressure, P**	**Phase fraction, α**	**Point displacement**
		BC	**BC**	**BC**	**BC**
Body	Wall	*movingWallVelocity uniform (0 0 0)*	*zeroGradient*	*zeroGradient*	*oscillatingDispl-acement*
Inlet	Patch	*zeroGradient*	*fixedFluxPressure uniform (0)*	*zeroGradient*	*fixedValue uniform (0 0 0)*
Outlet	Patch	*zeroGradient*	*fixedFluxPressure uniform (0)*	*zeroGradient*	*fixedValue uniform (0 0 0)*
Lower wall	Wall	*fixedValue uniform (0 0 0)*	*fixedFluxPressure uniform (0)*	*zeroGradient*	*fixedValue uniform (0 0 0)*
Atmosphere	Patch	*pressureInletO-utletVelocity uniform (0 0 0)*	*totalPressure uniform (0)*	*inletOutlet uniform (0)*	*fixedValue uniform (0 0 0)*
Front and Back	Empty	*empty*	*empty*	*empty*	*empty*

The *oscillatingDisplacement* boundary condition for point displacements on the body enforces sinusoidal motion with a set amplitude and frequency. The following twelve simulations are performed with oscillation frequencies equivalent to the wave periods used in the calculation linear wave forces.

Table 15. Forced heave oscillations

Oscillation period [s]	Oscillation frequency [rad/s]	Oscillation amplitude [m]
0,75	4,712	0,010
0,80	5,027	0,010
0,85	5,341	0,010
0,90	5,655	0,010
0,95	5,969	0,010
1,00	6,283	0,010
1,05	6,597	0,010
1,10	6,912	0,010
1,15	7,226	0,010
1,20	7,540	0,010
1,25	7,854	0,010
1,50	9,425	0,010

Hydrodynamic vertical forces on the body are calculated using the *forces* function objective, as described in previous sections. Amplitudes of 0.01m help to ensure that the measured forces are similar to linear potential theory predictions for the same case. This is indicated by the waves produced by the forced motions which are small and likely fall within the range of applicability for linear theory described in (Le Mehaute, 2013).

The measured hydrodynamic forces for each oscillation frequency may be broken down as follows.

$$F_{Hydro} = F_A + F_B + F_R$$

Where,

- F_A: Added mass force
- F_B: Damping force
- F_R: Restoring force

Added mass force is defined as the force exerted upon the body by the fluid in phase with the body's acceleration. The damping force is similar to the added mass force but rather in phase with the body's velocity. Restoring force is associated with changes in buoyancy due to varying hydrostatic pressure as the body moves vertically and is thus the force exerted on the body by the fluid in phase with body displacement.

Hydrodynamic force may then be written as

$$F_{Hydro,3} = -A_{33}\ddot{\eta}_3 - B_{33}\dot{\eta}_3 - C_{33}\eta_3$$

The negative signs are present because the hydrodynamic forces act in the opposite direction to the body motion. The linear restoring force coefficient is constant across all oscillation frequencies and given as

$$C_{33} = \rho g WPA$$

Frequency dependent added mass and damping coefficients are found using the hydrodynamic force equation with the measured force time series as follows.

The enforced heave motion is known to be

$$\eta_3 = \zeta_a sin\omega t$$

$$\dot{\eta}_3 = \omega\zeta_a cos\omega t$$

$$\ddot{\eta}_3 = -\omega^2\zeta_a sin\omega t$$

Expressions for the coefficients can then be formulated by multiplying the hydrodynamic force equation by the forced acceleration and the forced velocity respectively. They are then integrated over an integral number of oscillation periods to remove odd terms and rearranged as

$$A_{33} = \frac{-\int F_{Hydro,3}\,\ddot{\eta}_3 - C_{33}\int \eta_3\ddot{\eta}_3 dt}{\int \ddot{\eta}_3\ddot{\eta}_3 dt}$$

$$B_{33} = \frac{-\int F_{Hydro,3}\,\dot{\eta}_3}{\int \dot{\eta}_3\dot{\eta}_3 dt}$$

Integration limits have been selected for each case corresponding to a steady state region in the measured hydrodynamic force time series.

5.5 POST-PROCESSING

Simulations are first visualised using the third-party software ParaView in which a graphic interface provides oversight of the pressure, velocities and phase fractions terms at each time step.

Force values are written to a text file and subsequently processed using MATLAB. The post-processing technique for the 0.8T0.017H case from test 1 is provided as an example below.

Raw signals are filtered for noise and mean loads using cut-offs of 0.2 and 4 times the wave frequencies, as shown in figures 17 and 18. After initial filtering the resulting time series is named ‘Original’.

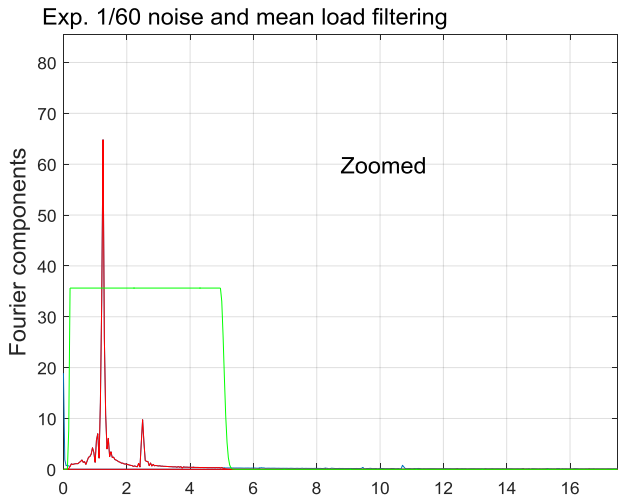

Figure 17. Noise and mean load by-pass filtering of experimental signal

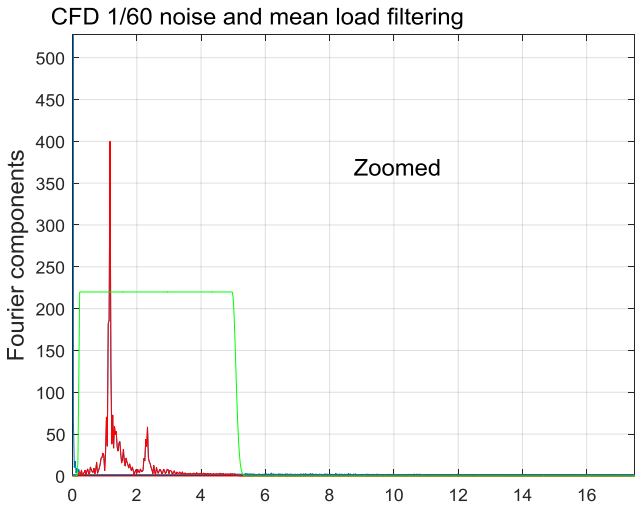

Figure 18. Noise and mean load by-pass filtering of CFD signal

It should be noted that the filtering program has been developed by the project supervisor, Trygve Kristiansen.

The second harmonic peaks are clearly visible in the frequency spectra above. Harmonic contributions are extracted using by-pass filtering around integer multiples of the wave frequency. Cut-off frequencies vary case by case but are generally set at less than +/-30% of the fundamental frequency away from the harmonic frequency. Figure 19 below provides an example of harmonic decomposition using the experimental and numerical forces.

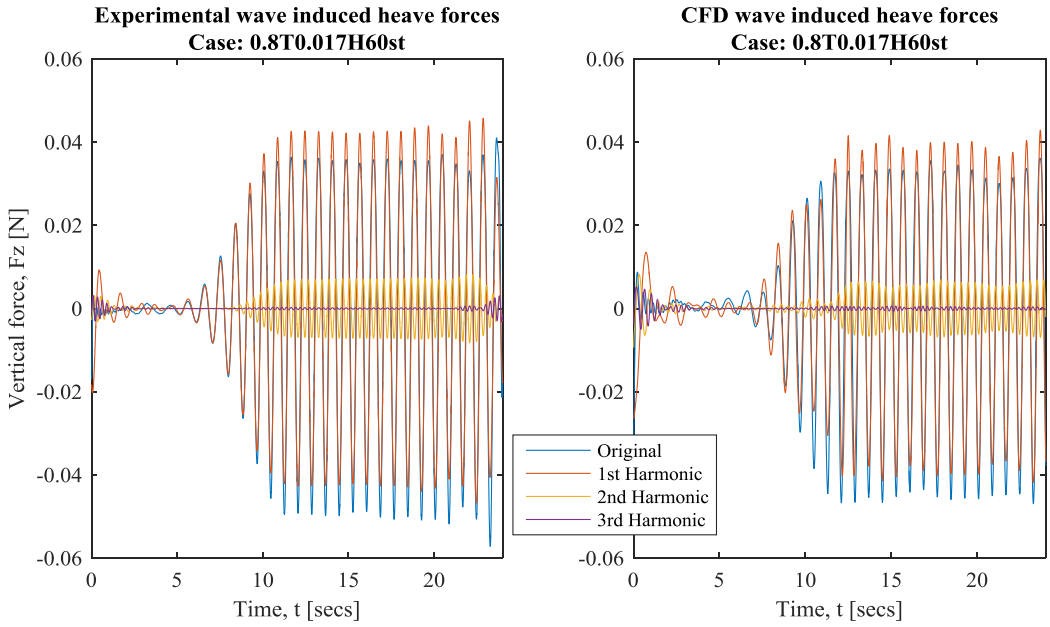

Figure 19. Harmonic decomposition

This process is repeated for each fixed simulation and harmonic contributions, taken as the average heights of each harmonic signal within steady state regions, are compared for the runs of tests 1, 2 and 3.

These average force values are non-dimensionalised using

$$\tilde{F} = \frac{F}{\rho g D^3}$$

Where,

- D: Characteristic length, taken as span of the buoy in x

Linear forces are obtained using the same method. Force filtering is applied to extract the first harmonics of the 1/200 steepness waves. Figure 20 presents the linear force filtering and the results time series for the 1.0 second period linear wave.

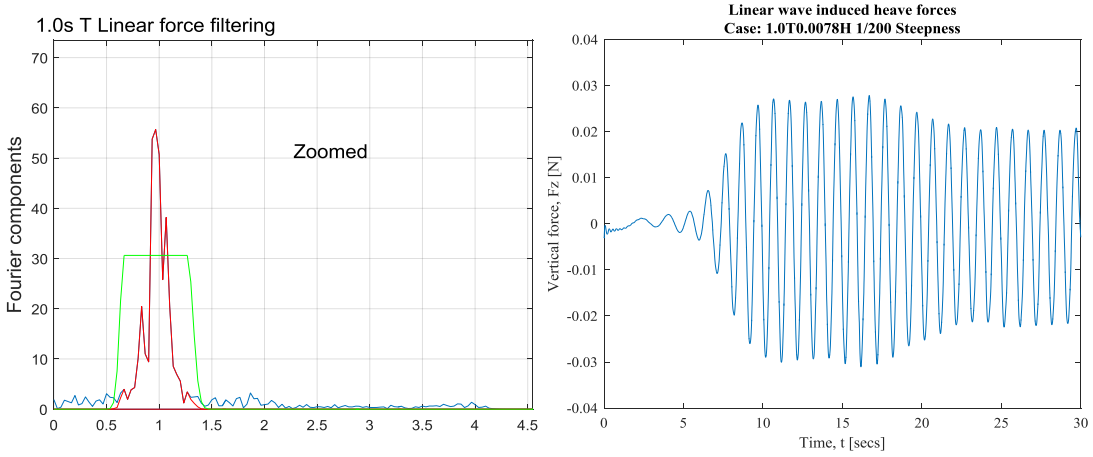

Figure 20. Development of linear force time series

Scaling of linear forces, for comparison with numerical and experimental tests 1, 2 and 3, is achieved by calculating a scale factor as

$$SF = \frac{desired\ steepness}{linear\ steepness} = 200\,{}^{H}/_{\lambda}$$

For post-processing floating case simulation, orientation values for the buoy's centre of mass are extracted and input to MATLAB. The first harmonics of each CFD response are compared to linear responses calculated using the linear simulator described previously. First

harmonic extraction from response time series is achieved in an identical manner to that described for forces. 1st harmonic responses are then non-dimensionalised into response amplitude operators (RAOs), describing the response per unit amplitude of an appropriately scaled linear wave. In this we they may be compared against linear response RAOs.

6 RESULTS AND DISCUSSION

6.1 WAVE INDUCED FORCES ON A FIXED BUOY

Results for the experimental and numerical fixed case tests are compared in the following section and examined with respect to linear force calculations.

6.1.1 Test 1: Regular incident waves with 0.8 second periods

Non-dimensional load harmonics of the four experimental and numerical runs in test 1 are plotted in figure 21 along with forces corresponding to linear theory. Values correspond to the average heights of force oscillations taken from steady state regions in each harmonic contribution's time series. Force results are non-dimensionalised as follows,

$$\tilde{F} = \frac{F}{\rho g D^3}$$

For more details on the post processing techniques employed the reader should refer to section 5.5.

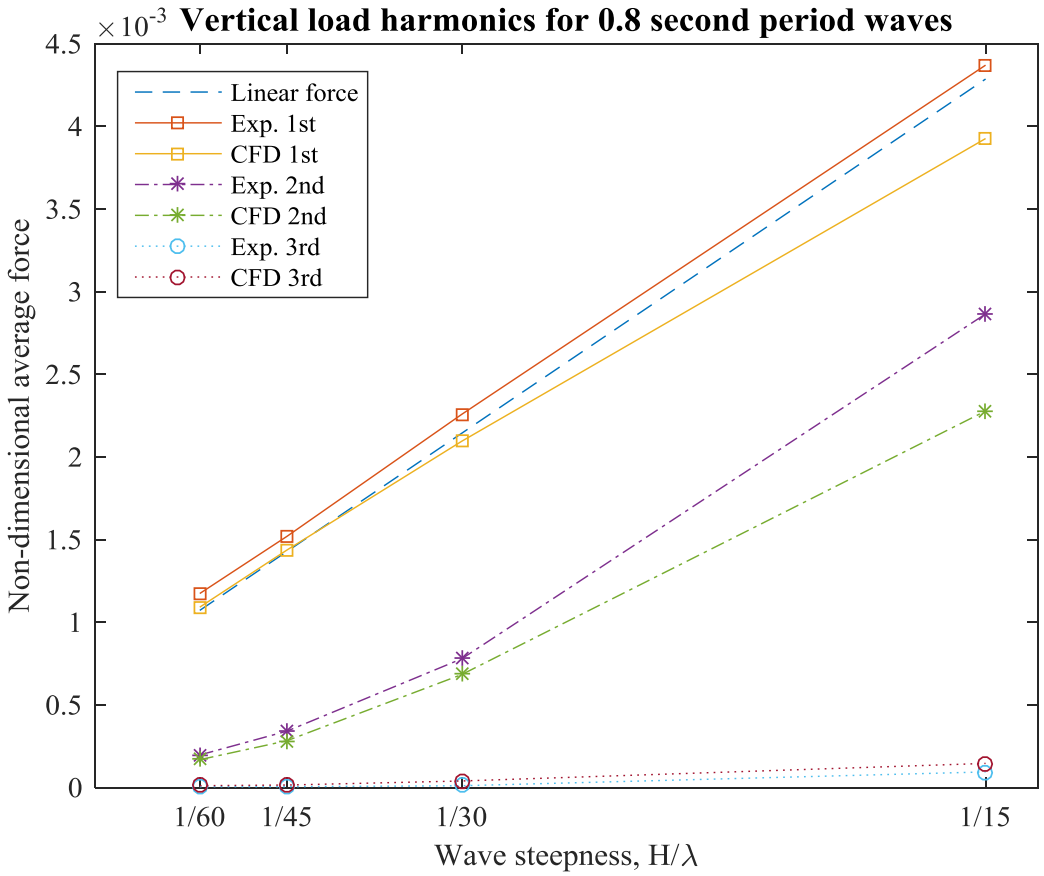

Figure 21. Test 1- Force harmonics

It is of interest to comment on the validity of numerical results with reference to experimental measurements. Experimental results carry greater magnitude across all 1st and 2nd harmonics for each wave steepness however errors are mostly consistent up until 1/15 wave steepness. A probable cause of the lower numerical values is the inability of the inlet boundary conditions to generate desired wave heights to a high level of accuracy and also the presence of numerical wave damping, as observed in the mesh study presented in section 5.1.3. Good agreement in shape between experimental and numerical results is seen for wave steepness less than and equal to 1/30 with discrepancy remaining relatively constant at under 7.2% in 1st harmonics. Divergence however is seen for the 1/15 case in which the CFD harmonics are substantially lower than experimental values, with discrepancy of 10.2% in the 1st and 20.5% in the 2nd harmonic.

A main consideration for the presented project is linear theory's potential to model wave loads. Clearly from figure 21, linear theory can only model 1st harmonic loading and it does this successfully for the entire experimental test, predicting the same trend but with a

smaller magnitude. CFD 1st harmonics follow linear estimations almost perfectly up until 1/15 wave steepness where experimental values follow the linear relation but CFD values are reduced. To investigate this drop in CFD 1st harmonic values it is useful to visualise both the experimental and numerical runs in figures 22 & 23.

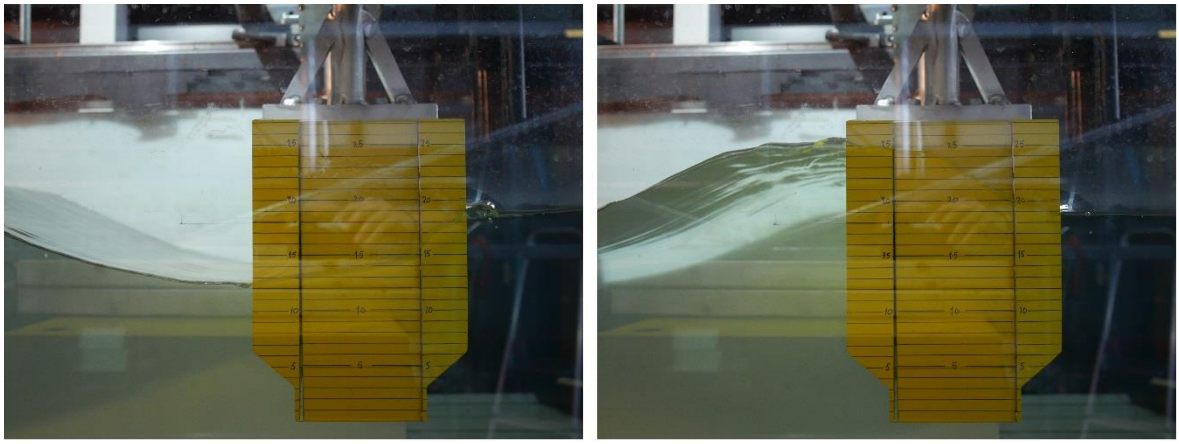

Figure 22. Experiment- 0.8T0.067H 1/15 steepness

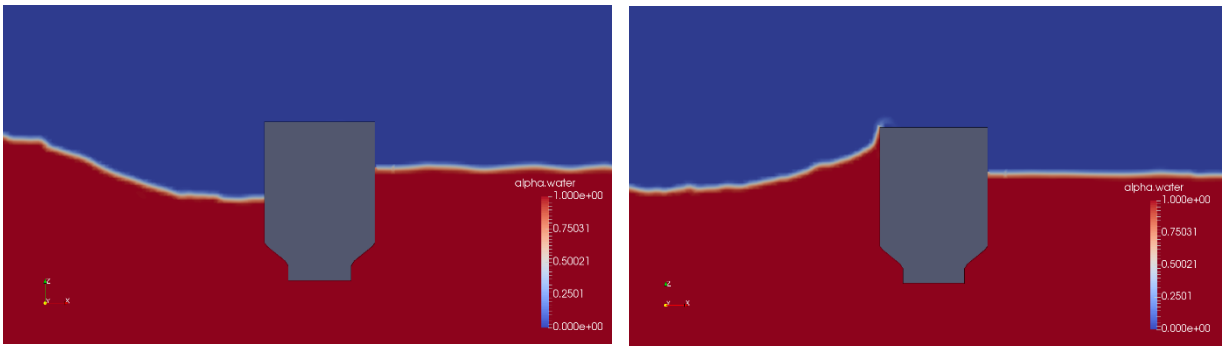

Figure 23. InterFoam- 0.8T0.067H 1/15 steepness

A small amount of overtopping is observed in the numerical simulation but not in the experimental run. This could be a contributing factor to the reduction in the numerical first harmonic as loads acting in negative z are experienced for each wave period thus affecting forces oscillating at the fundamental frequency.

2nd harmonics in both the numerical and experimental forces are of significance for all wave steepness and dominate the higher order contributions as 3rd harmonics are of little significance. Numerical values are shown in table 16 where magnitudes are given as percentages of the 1st harmonics.

Table 16. Test 1- CFD 2nd order harmonics

Wave steepness, H/λ	2nd harmonic (% of 1st)
1/60	15,4
1/45	19,7
1/30	32,6
1/15	58,0

The effect of 2nd harmonic loads can be illuminated when comparing CFD and linear force time series in figure 24. CFD forces are referred to here as 'CFD Original' forces and of comprised of raw data with noise and mean loads removed.

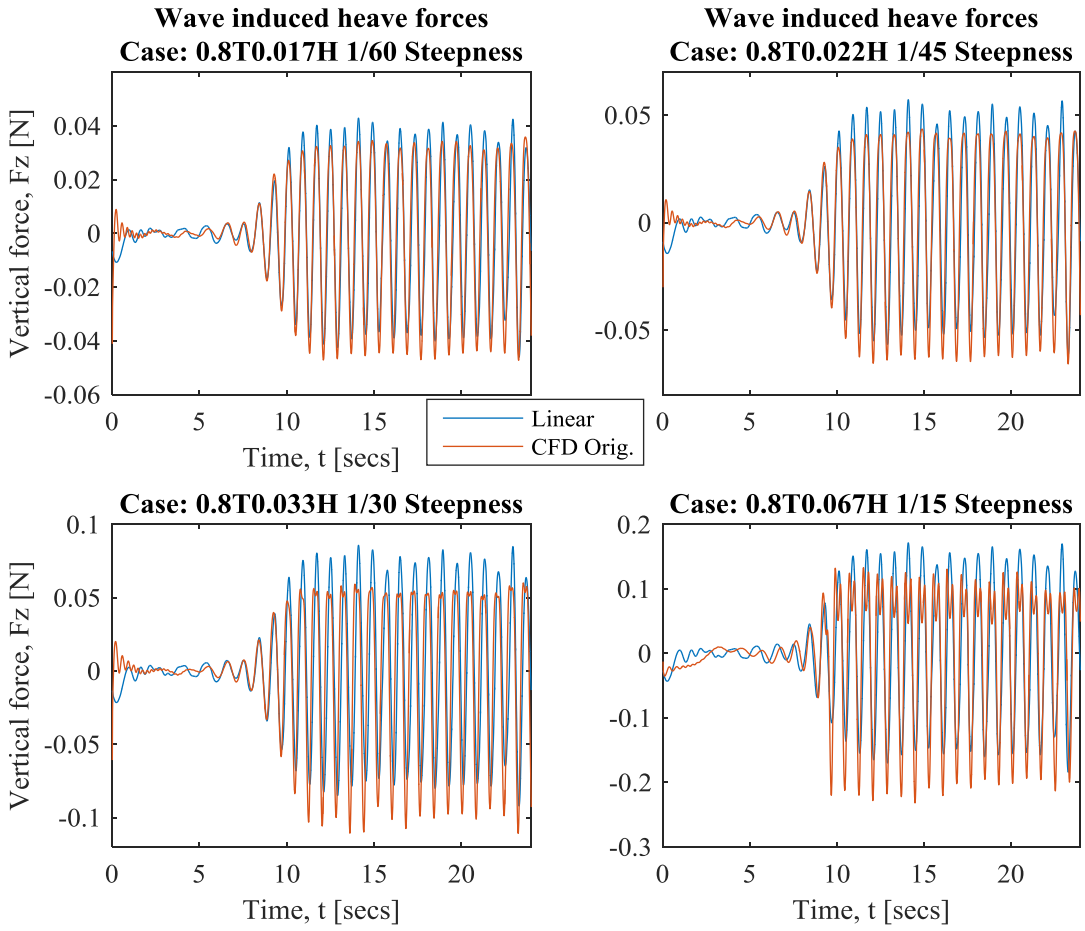

Figure 24. Test 1- CFD and linear time series

The 2nd order harmonics oscillating at twice the fundamental wave frequency act to reduce the maxima of oscillations and for high steepness cases this produces secondary peaks. To show this more clearly the 1/15 CFD force is presented below.

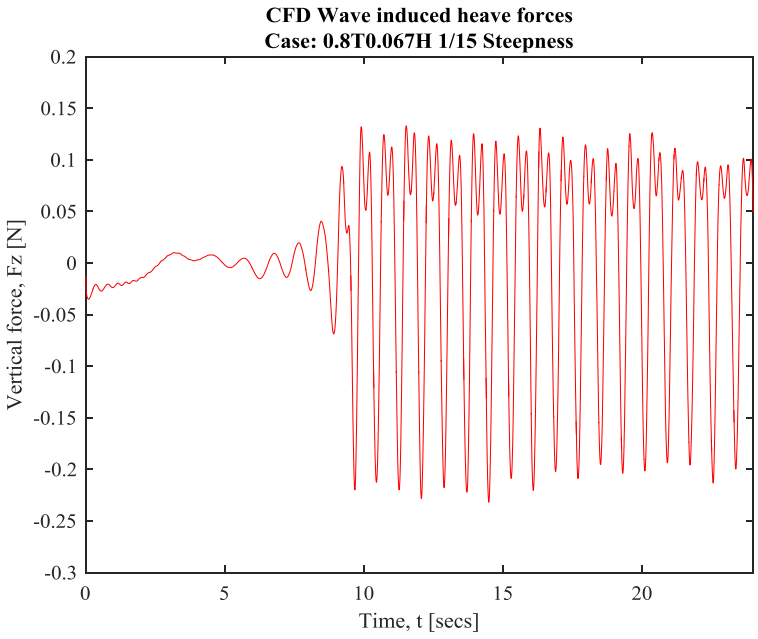

Figure 25. Case: 0.8T0.067H 1/15 Steepness- CFD force time series

By plotting the 1st and 2nd harmonics which as seen in figure 21 are the majority contributors to the above force one can attempt the shape of the original force is formed. As shown in figure 26, the 2nd harmonic has a trough at each of the 1st harmonic crests, by adding the two series it is easy to imagine the resulting shape to be similar to that of figure 25.

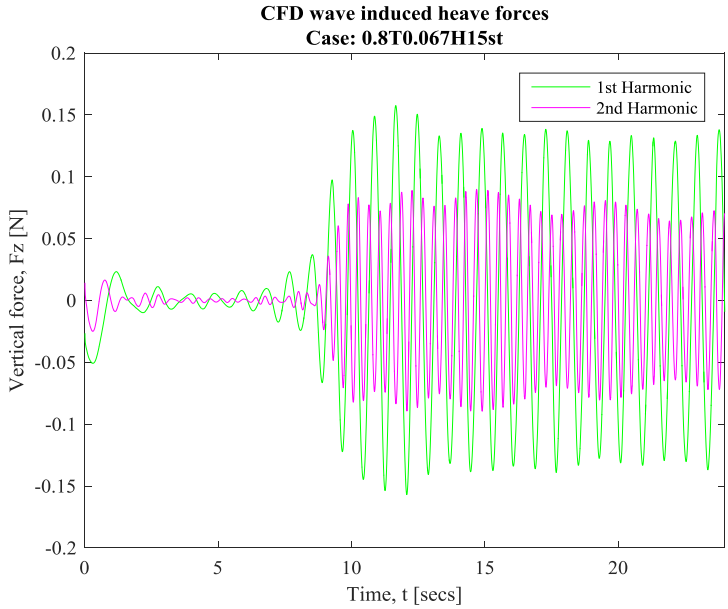

Figure 26. Case: 0.8T0.016H 1/15 Steepness- CFD 1st and 2nd harmonic force time series

6.1.2 Test 2: Regular incident waves with 1.0 second periods

Figure 27 presents the non-dimensional load harmonics for test 2 with corresponding linear forces.

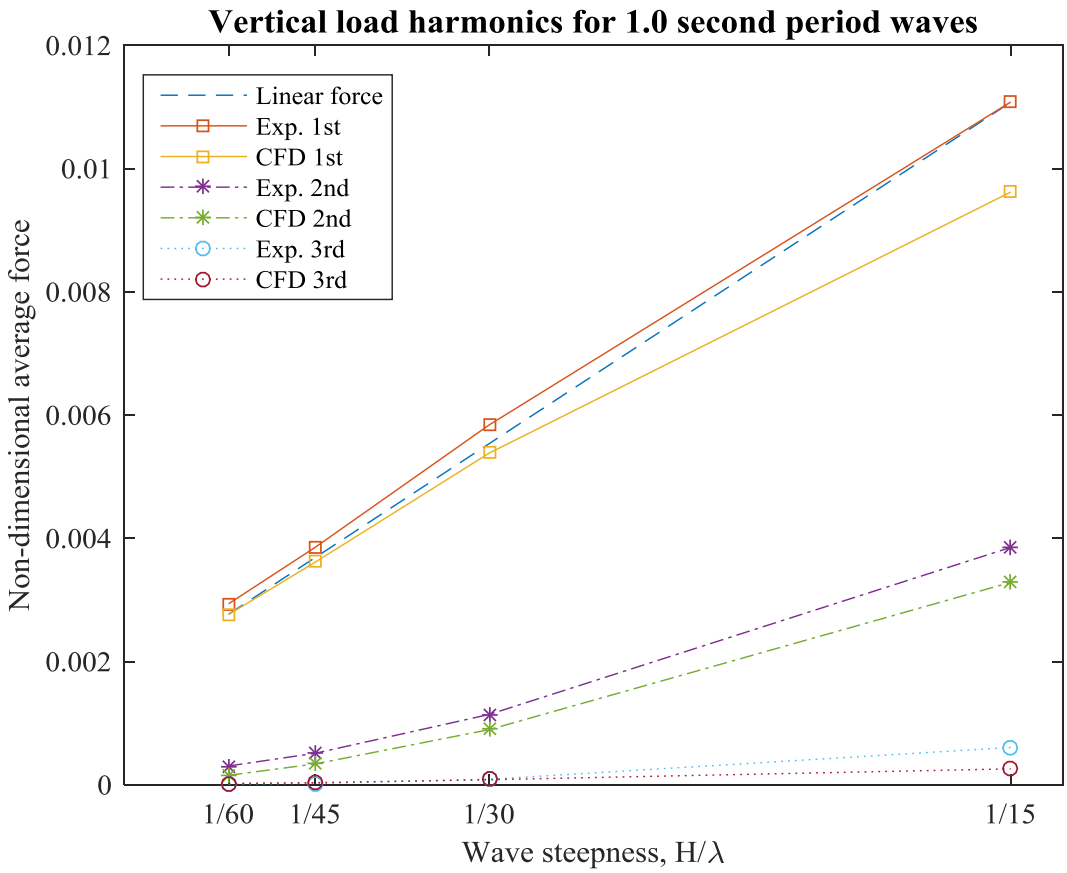

Figure 27. Test 2- Force harmonics

The trends in experimental and numerical results show agreement in shape across all harmonics. Once again experimental results carry greater magnitude but errors are consistent and likely due to the wave modelling performance of the numerical setup. 1st harmonics follow linear relations until 1/15 wave steepness cases, in which overtopping is present during experimental and numerical runs, as shown in figures 28 & 29.

Figure 28. Experiment- 1.0T0.104H 1/15 steepness

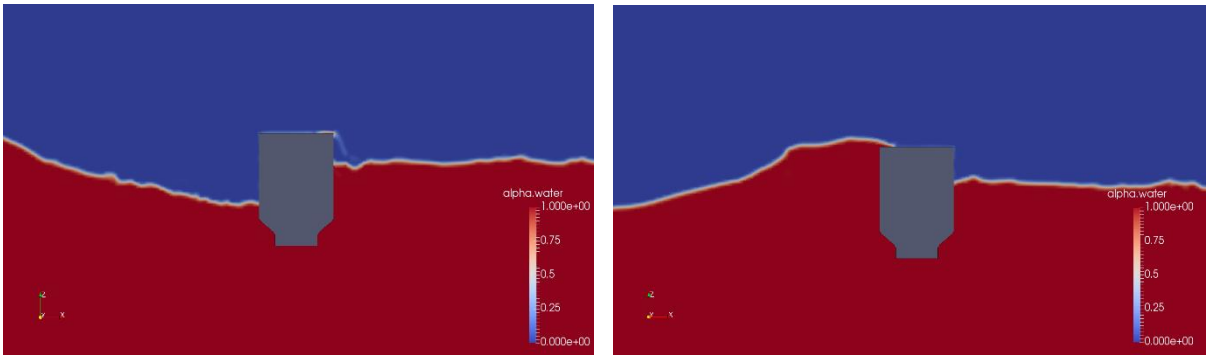

Figure 29. InterFoam- 1.0T0.104H 1/15 steepness

2nd order harmonics have considerable magnitudes and 3rd harmonics are negligible. The magnitude of numerical second order forces are presented in table 17.

Table 17. Test 2- CFD 2nd order harmonics

Wave steepness, H/λ	**2nd harmonic (% of 1st)**
1/60	5,6
1/45	9,4
1/30	16,7
1/15	34,2

By comparing linear and CFD forces it is observed that the effect of these second order contributions is similar to those observed in test 1 but to a lesser extent.

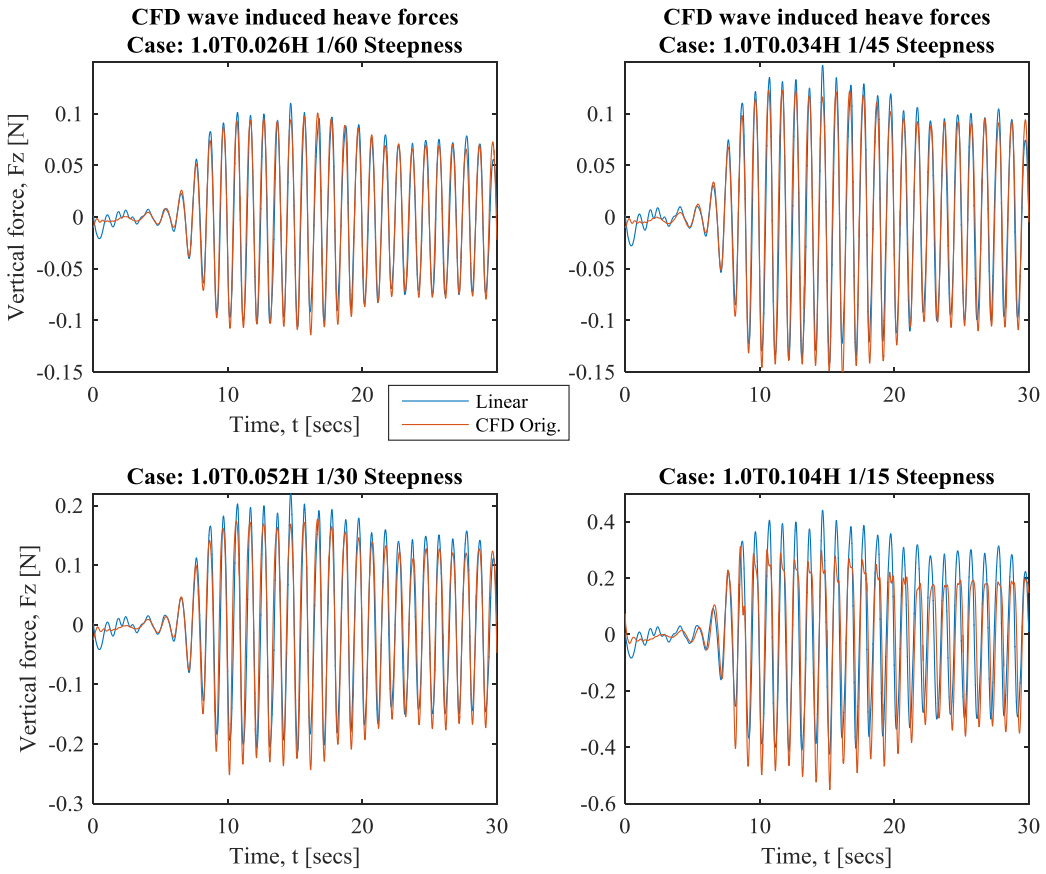

Figure 30. Test 2- CFD and linear time series

6.1.3 Test 3: Regular incident waves with 1.2 second periods

Force harmonics extracted from experimental and numerical runs in test 3 plus associated linear forces are provided in figure 31.

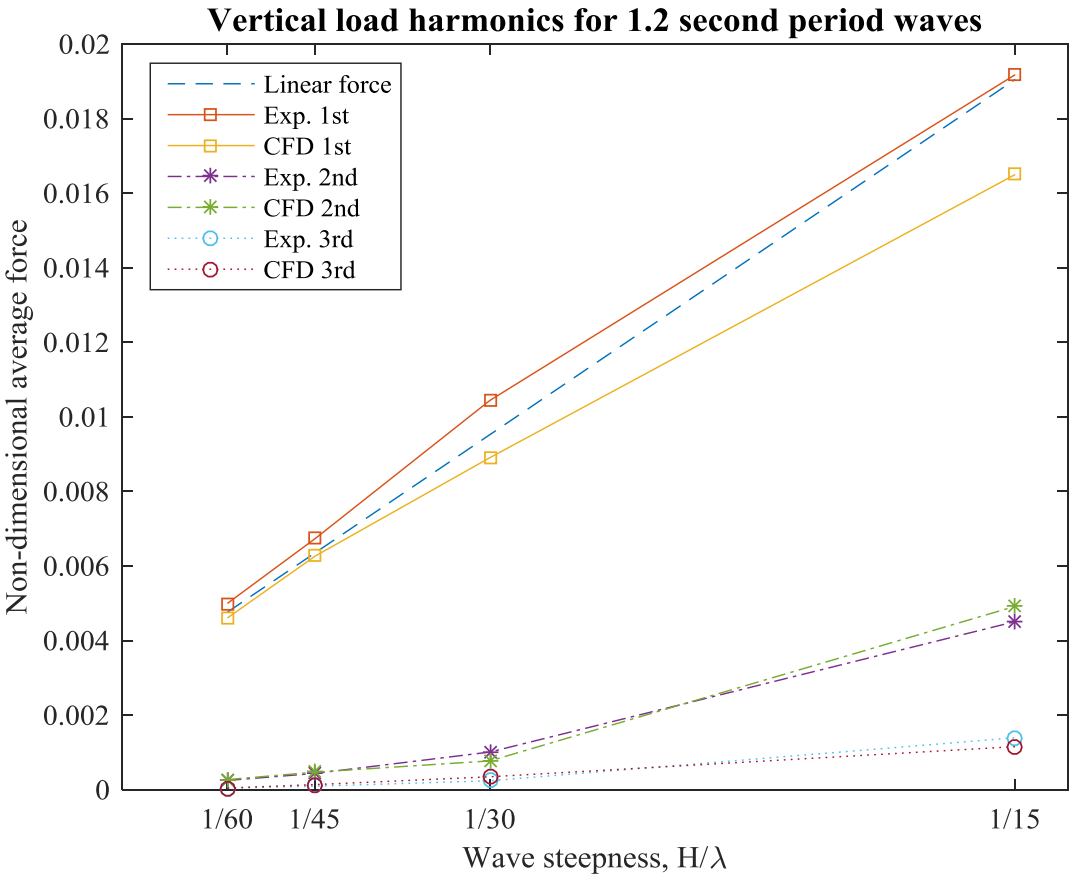

Figure 31. Test 3- Force harmonics

Greater disagreement in trends is observed between experimental and numerical results than in previous tests. Numerical 1st harmonics only agree with linear theory up to 1/45 whereas experimental results have a linear relation up to 1/30. Once again it is interesting to visualise the experiments and simulations, to identify if overtopping is a contributing factor to this inconsistency.

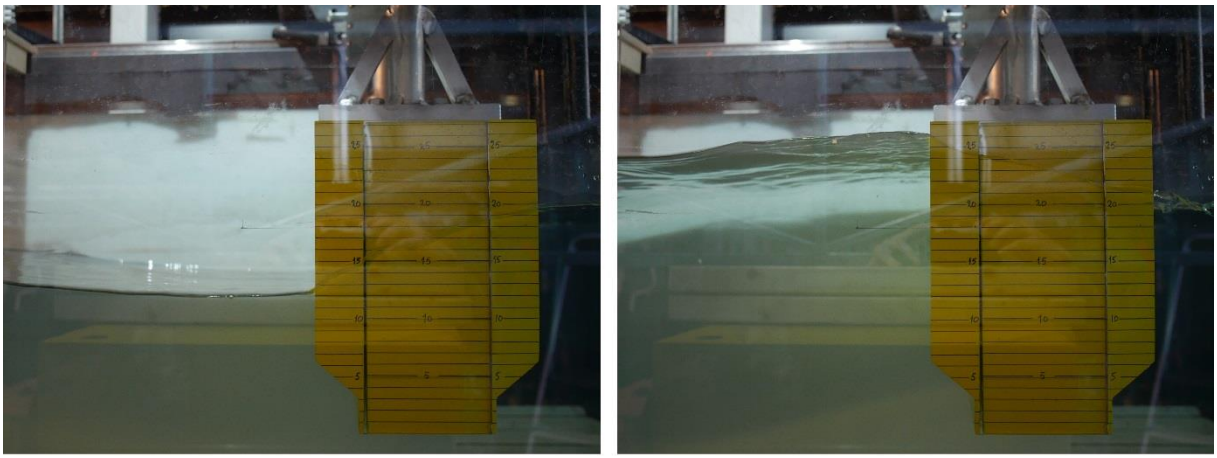

Figure 32. Experiment- 1.2T0.074H 1/30 steepness

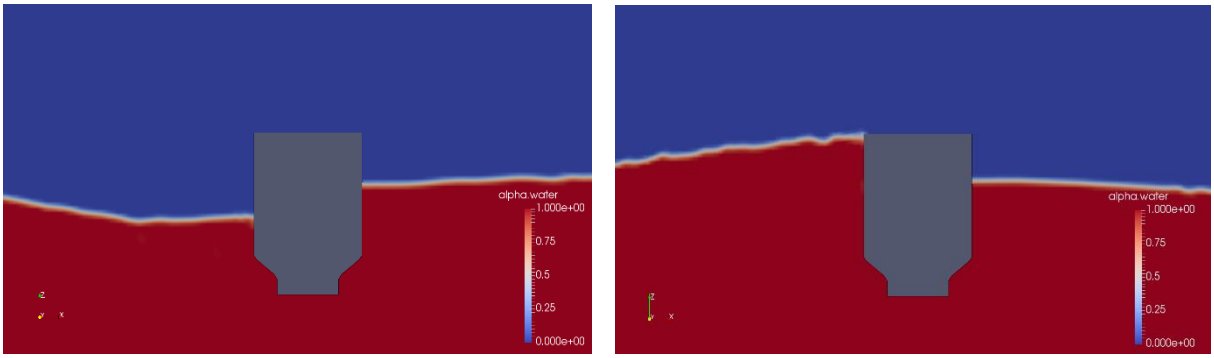

Figure 33. InterFoam- 1.2T0.074H 1/30 steepness

Figures 32 and 33 depict no overtopping with 1/30 steepness waves in experiments however a small amount is observed in numerical simulations.

Figure 34. Experiment- 1.2T0.149H 1/15 steepness

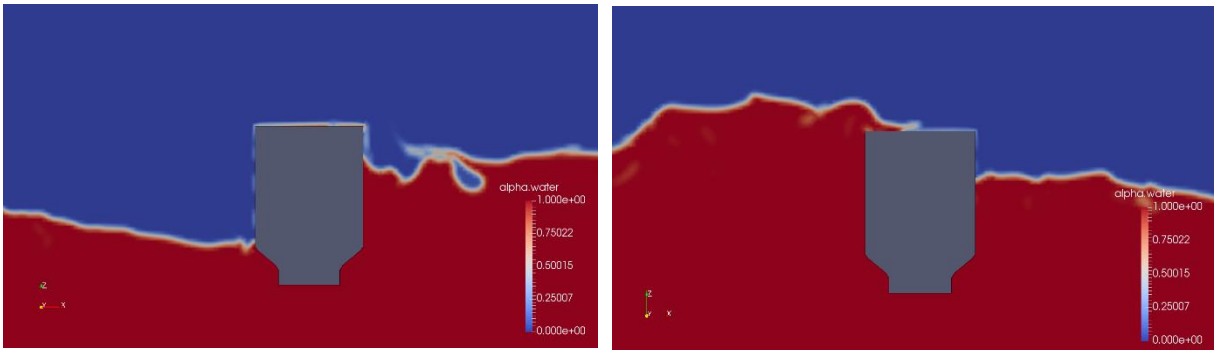

Figure 35. InterFoam- 1.2T0.149H 1/15 steepness

Extensive overtopping is seen in figures 34 & 35, detailing numerical and experimental runs in which the WEC buoy is exposed to 1/15 steepness waves with 1.2 second periods.

The analysis above provides another suggestion that overtopping acts to reduce first harmonic contributions and gives a possible explanation of the disagreement in shape seen between experimental and numerical first harmonic plots in figure 31.

In comparison to the previous tests, CFD second order contributions for the 1.2 second period waves, provided in table 18, are less significant. Once again 3rd harmonics carry only small amplitude. This is particularly obvious for the 1/30 steepness case.

Table 18. Test 3- CFD 2nd order harmonics

Wave steepness, H/λ	**2nd harmonic (% of 1st)**
1/60	5,9
1/45	7,5
1/30	8,7
1/15	29,8

Comparing linear forces with CFD original time series, in figure 36, one sees better agreement than in previous tests.

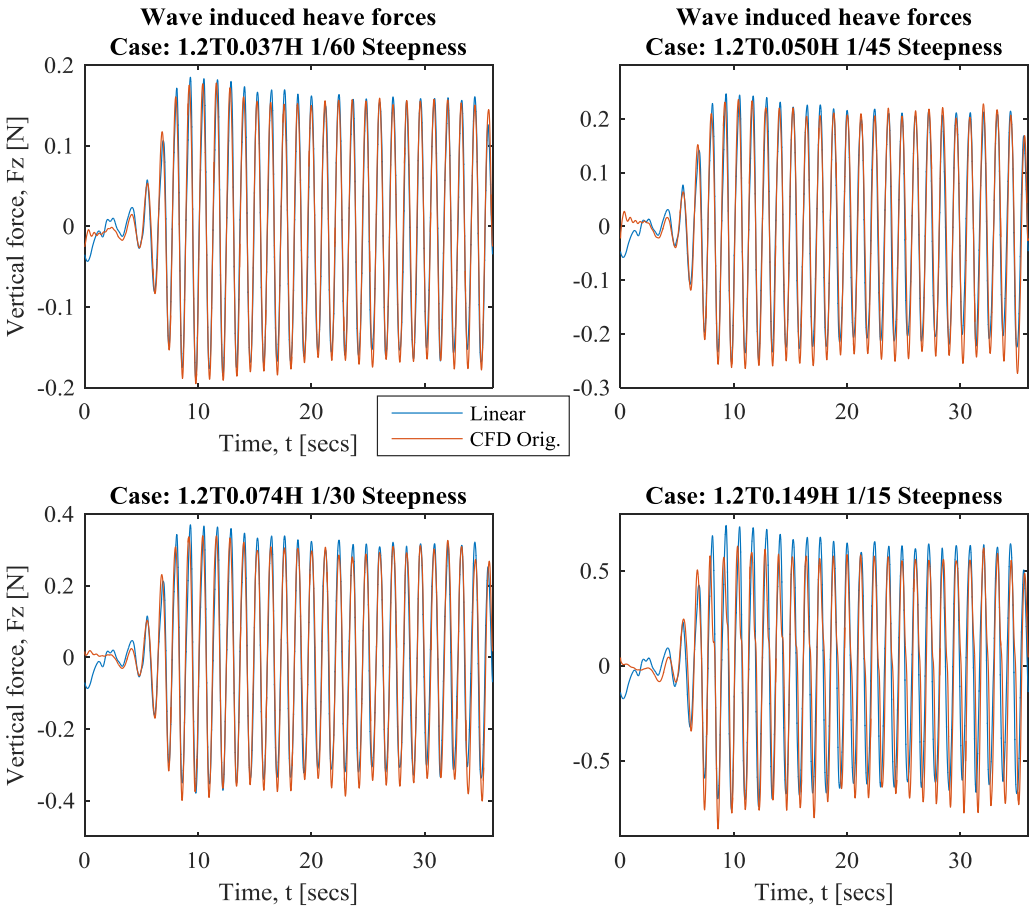

Figure 36. Test 3- CFD and linear time series

While second order contributions reduce the maximum height of oscillations, most prominently for 1/15 steepness waves, the shape is similar to linear forces for all cases.

For comparison with test 3, (Chen et al., 2014) provides a detailed investigation of wave-structure interactions between vertical surface piercing cylinders and regular waves. CFD simulations of a 1/15 steepness wave with 1.22 second period waves, were performed with results comparing well to experimental data. (Chen et al., 2014) remarked that "steeper waves lead to stronger nonlinear wave-structure interactions and more significant nonlinear effects", finding that for wave-loading on the cylinder, harmonic contributions of order greater than 1 had a magnitude equal to 31% of the 1st harmonic for the 1/15 steepness wave, showing close agreement with the presented study.

* * *

On inspection of the three tests above one observes reasonable agreement between experimental data and numerical results. In general, experimental values produce higher magnitude forces for each tested wave steepness however plot shapes and relations remain consistent with numerical results. This is particularly apparent at low steepness i.e. for the 1/60 and 1/45 cases, where discrepancy between numerical and experimental first harmonics remains at roughly 8%. Disagreement however is introduced for steep cases; overtopping develops earlier in numerical simulations for tests 1 and 3. This coincides with divergence of CFD values from experimental results. One can say that the experimental results suggest validity of the low steepness numerical forces but that there is a level of uncertainty around high steepness cases. A likely cause for lower numerical results is the wave generating ability of the numerical setup and earlier overtopping may be due to mesh characteristics exaggerating wave diffraction and effecting free-surface positioning.

It is clear on inspection of the harmonic plots that linear forces consistent have the capacity to model 1st harmonics with a good level of accuracy at low wave steepness. When examining linear force predictions, one sees very good agreement with numerical results and consistency in shape with experimental data for up to 1/30 steepness in tests 1 and 2 and 1/45 in test 3. The initiation of overtopping is concurrent with deviation of the first harmonics from linear theory for both experimental and numerical runs. The findings infer that linear forces can only model the first harmonics accurately in cases where overtopping is not present.

Higher harmonic forces are apparent for all fixed body cases and increase with wave steepness, for the presented studies 3rd harmonics share the same trend but have small magnitudes and are not examined further. An obvious trend observed is that greater contributions are prevalent in tests with shorter periods; 2nd harmonic contributions are largest for high steepness waves with short periods, such as the 1/15 case in test 1. In tests 1 and 2 a parallel relation is seen; second harmonic contributions remain similarly low for 1/60 and 1/45 steepness then become prominent at 1/30 before roughly doubling for 1/15 waves. In test 3 however 2nd harmonics only become prominent for 1/15 waves. These forces, oscillating at double the wave frequency, act to alter the shape of first harmonic force time series, reducing maxima and creating additional peaks, most prominently for high steepness, low period cases. This reduces linear theories capacity to estimate forces when higher order contributions are present. For many scenarios, such forces require analysis as they can be of key concern to structural loading, fatigue damage as well as high frequency resonant response motions and

therefore state of the art numerical techniques for modelling wave forces based on linear potential flow theory are insufficient.

6.2 HEAVE RESPONSE OF A FLOATING BUOY

Using methods described in chapter 5 a linear response RAO plot has been produced for comparison with floating heave responses measured in CFD simulations using the *InterDyMFoam* solver. This section first presents the linear hydrodynamic coefficients required for computed linear responses and identifies the natural frequency of the buoy in heave before numerical and linear response values are plotted and examined.

6.2.1 Linear hydrodynamic coefficients

The linear restoring coefficient in heave remains constant for all wave periods and is given below.

$$C_{33} = 19.1295$$

Frequency dependent added mass and damping terms are presented in table 19 for oscillatory periods ranging from 0.75 to 1.5 seconds.

Table 19. Linear hydrodynamic coefficients

Period, T [secs]	Added mass coefficient, A33	Wave damping coefficient, B33
0,75	0,134	0,285
0,8	0,127	0,338
0,85	0,123	0,382
0,9	0,120	0,387
0,95	0,118	0,502
1	0,114	0,506
1,05	0,115	0,543
1,1	0,120	0,577
1,15	0,121	0,564
1,2	0,113	0,581
1,25	0,103	0,625
1,5	0,127	0,606

When considering response of the structure it is of interest to consider the natural period of the system, and thus the wave frequency at which the buoy's heave response should theoretically be greatest. This is achieved using the added mass coefficients computed during the forced motion simulations with the following expression.

$$\omega_n = \sqrt{\frac{C_{33}}{m + A_{33}(\omega)}}$$

By plotting both the RHS expression using the 12 added mass values and a linear relation for the LHS, the natural frequency may be extracted from the intersection point, as shown in figure 37.

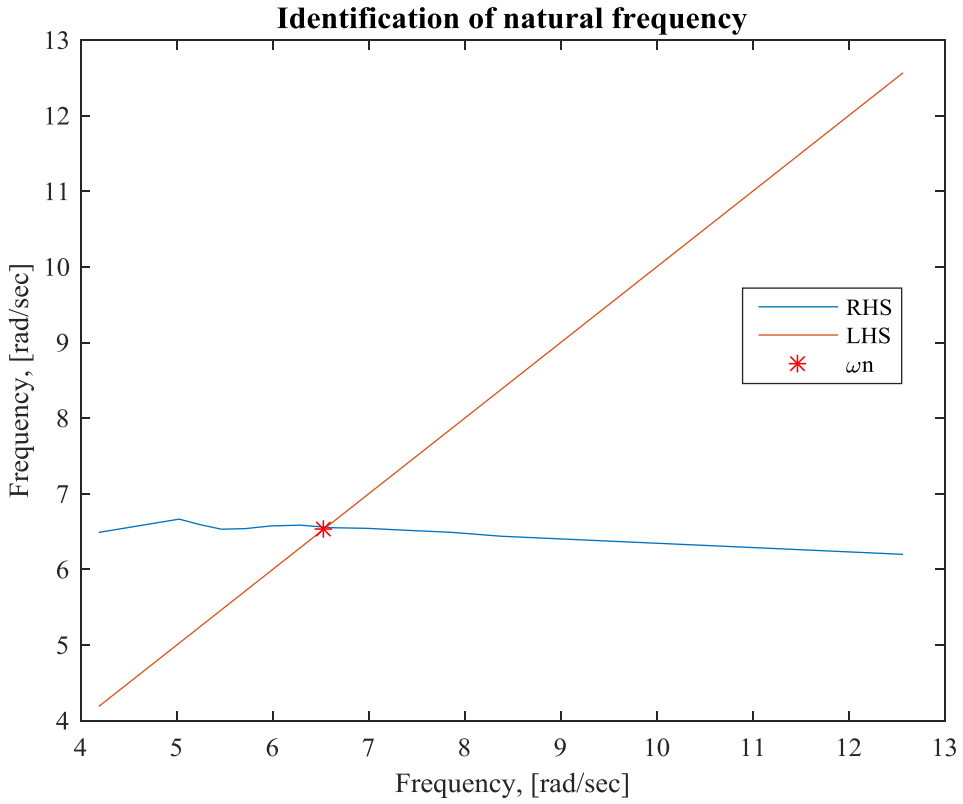

Figure 37.Plotting of natural frequency

Yielding a natural frequency of 6.527 rad/sec and a natural period of 0.9626 seconds. As this value is close to the fundamental wave frequencies used in the floating simulations it is unlikely that higher order harmonic responses will be excited, whereas if it were at double the wave frequency then resonance could be initiated by second order load harmonics and response at twice the wave frequency would be observed. In the present study, it is therefore assumed that 1st order harmonic behaviour will dominate, making comparisons with linear predictions of considerable interest.

6.2.2 Response

Twelve linear response RAOs for the 1/200 steepness waves are presented in figure 38, describing the amplitudes of response per unit linear wave height. The linear response values at wave periods 0.8, 1.0 and 1.2 seconds are plotted against RAOs computed from the 1st harmonic responses of the floating case CFD simulations. The natural frequency is included for reference as the wave frequency for which response motions are predicted to be greatest.

Note that the response values, used to compute RAOs, correspond to the average motion oscillations in steady state regions.

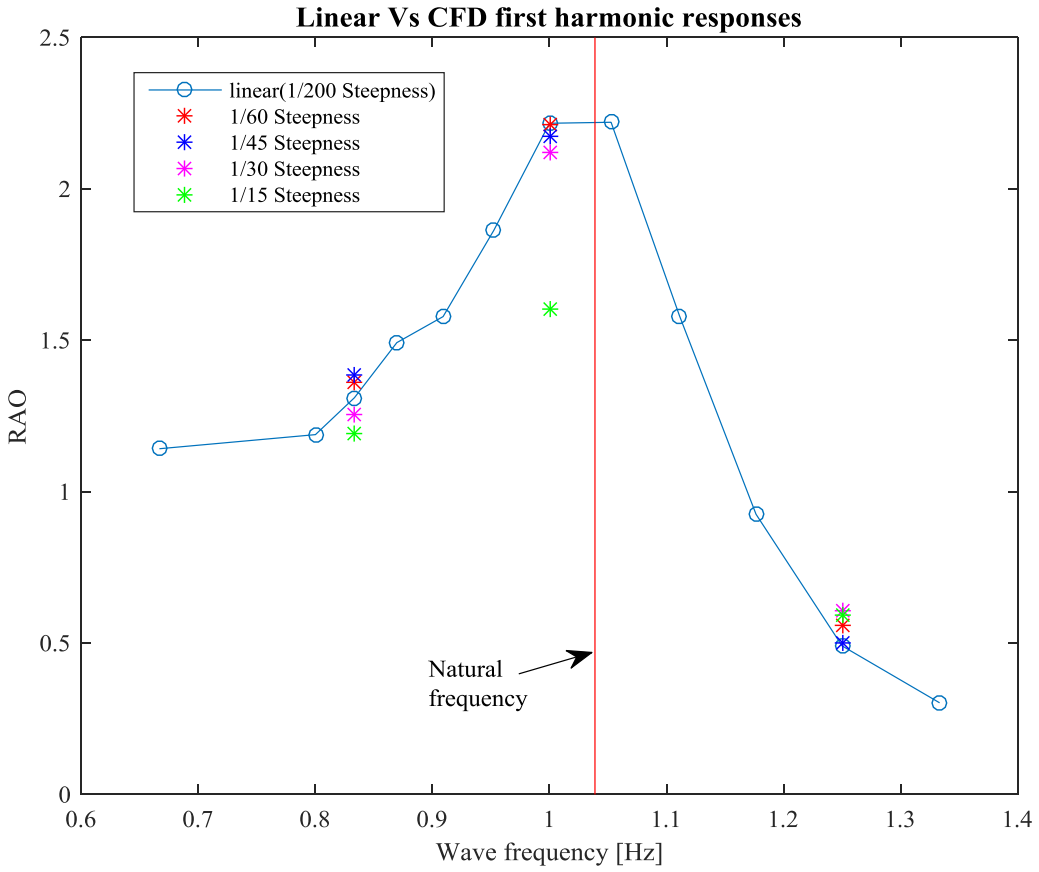

Figure 38. Wave induced responses

Reasonable agreement is shown between linear predictions and CFD 1st harmonic responses for all wave cases with periods away from resonance and up to the 1/30 case close to resonance. Relative to these, the 1/15 case near resonance is poorly modelled by linear theory with a discrepancy of 27.7%, measured as difference over the linear value.

The results of floating simulations with wave periods of 1.0 seconds, i.e. close to the natural period, display signs of beating, where force maxima and minima fluctuate in an oscillatory manner. This is characteristic of response near resonance and is shown in figures 39 & 40.

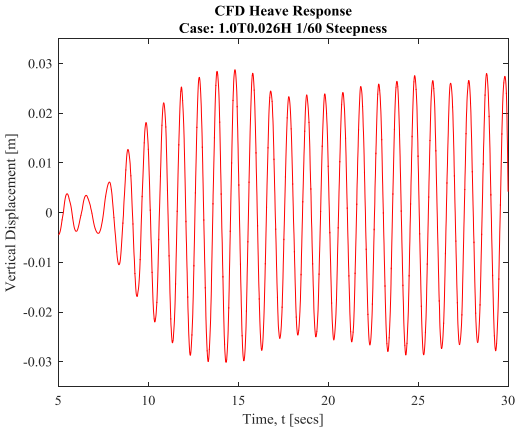

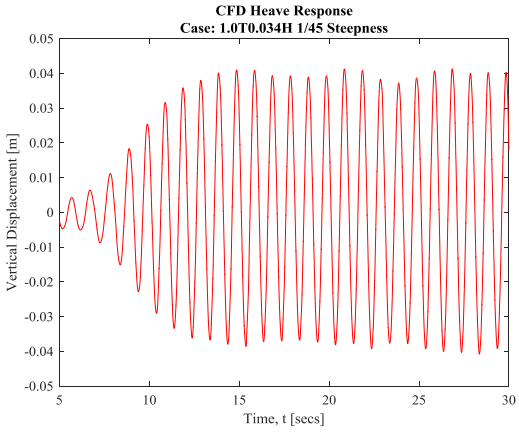

Figure 39. (L) Case: 1.0T0.026H 1/60 Steepness- Response

Figure 40. (R) Case: 1.0T0.034H 1/45 Steepness-Response

Although linear theory fails to predict this shape, for the 1/60, 1/45 and 1/30 steepness cases it produces similar average heights, as reflected in figure 38.

It is of interest to compare the 1/30 and 1/15 cases with 1 second wave period to distinguish any features that may cause poor linear estimation in the latter. Firstly, the linear and CFD response time series are presented in figures 41 & 42.

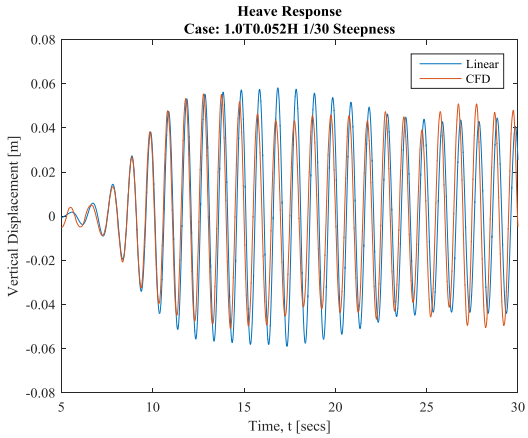

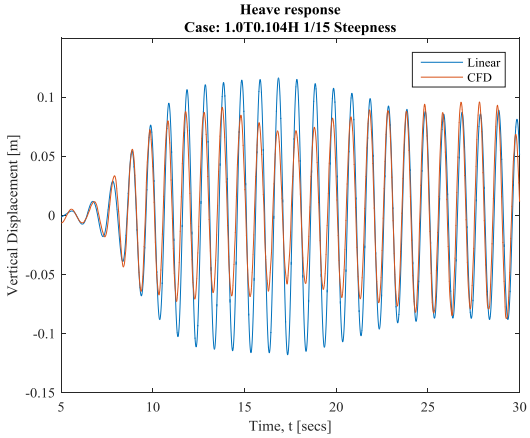

Figure 41. (L) Case: 1.0T0.052H 1/30 Steepness- Response

Figure 42. (R) Case:1.0T0.104H 1/15 Steepness- Response

Linear predictions drastically overshoot the CFD values in the steeper case. Typical behaviour in each simulation is visualised below.

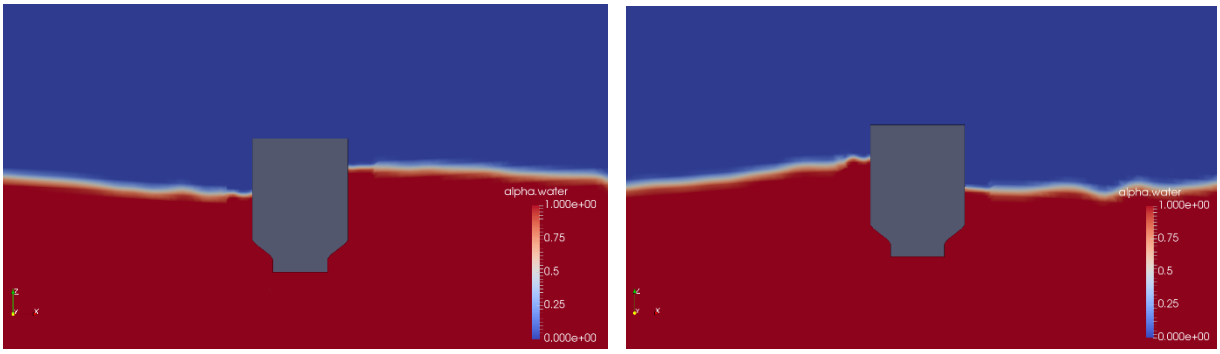

Figure 43. InterDyMFoam- 1.0T0.052H 1/30 Steepness

Overtopping is not observed in the 1/30 case shown above. With 1/15 waves however, violent wave behaviour and overtopping occurs, as shown in figure 44.

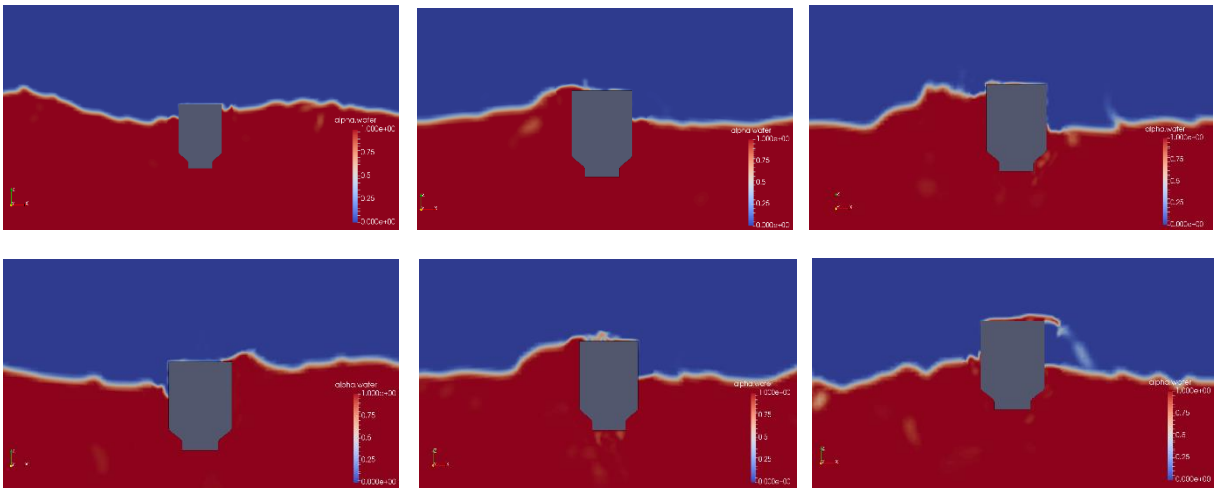

Figure 44. InterDyMFoam- 1.0T0.104H 1/15 Steepness

Analysis of cases with periods away from the natural period, overtopping is seen to a very small extent in the 0.8T0.067H 1/15 floating simulation and substantially in the 1.2T0.149H 1/15 case, as depicted in figures 45 &46.

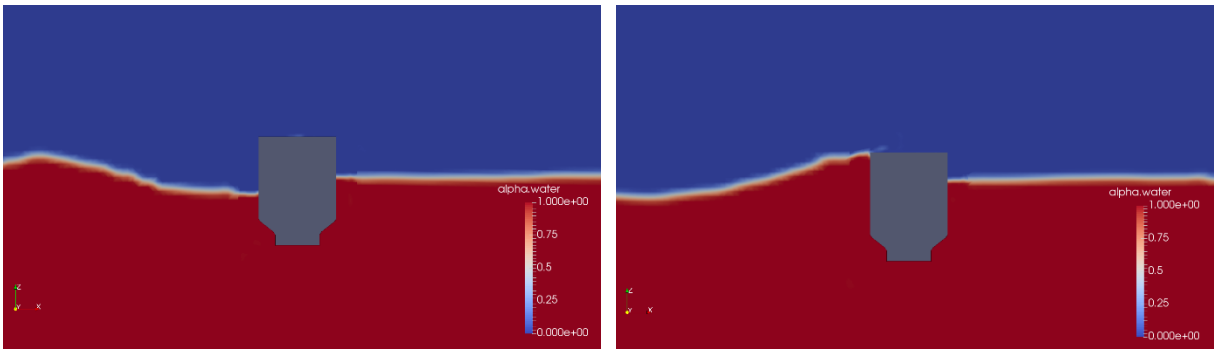

Figure 45. InterDymFoam- 0.8T0.067H 1/15 Steepness

Such wave breaking seems to have no damping effect on motions in figure 38.

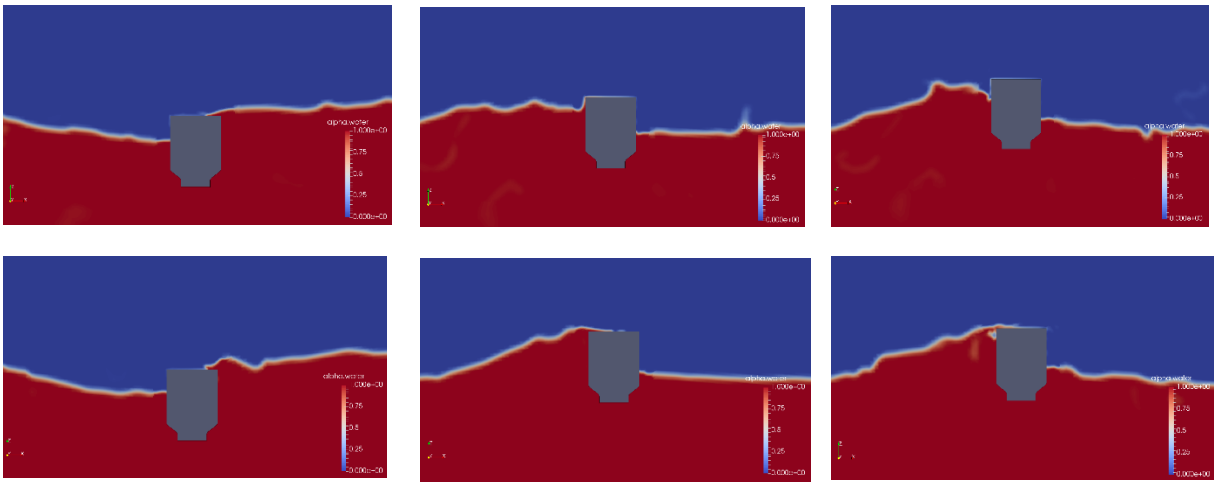

Figure 46. InterDyMFoam- 1.2T0.149H 1/15 Steepness

Although overtopping is extensive in figure 46, it seems to only have a small damping effect on motions induced by 1.2 second period waves, and response results are not far from linear predictions.

All cases that have not been individually presented involve no overtopping and motions are modelled well by linear theory.

The author suggests that such overtopping acts to damp the large amplitude motions experienced at frequencies close to resonance, contributing to reduced RAOs value when compared to linear estimations. Several other factors are of considerable importance which influence damping of motions, most notably viscous pressure forces caused by flow separation in boundary layers and vorticity in the surrounding fluid. Such effects would likely be observed for all large amplitude motions; however, it is only in the overtopping case close

to resonance where extensive damping occurs, thus their influence is reasoned to be of secondary importance.

From the presented study of responses linear theory clearly has good potential for modelling 1st harmonic responses of the buoy, however for large steepness waves, motion damping is experienced causing linear theory over estimations. This is most pronounced when overtopping is extensive and wave periods are close to resonance. Such results are consistent with an assessment made by (Ye Li and Yi-Hsiang Yu, 2012), recounting that frequency domain potential flow codes based on linear and weakly non-linear theory produce barely acceptable results close to resonance.

7 CONCLUSIONS

On completion of the presented project the following conclusions can be drawn regarding hydrodynamic analysis of the 2D WEC buoy section:

- Linear theory performs well in estimating CFD heave responses for wave periods away from the natural period. However, performance reduces for steep waves with periods close to resonance where overtopping is prevalent.
- Linear forces show good agreement with the first harmonic loads computed in CFD fixed case simulations for regular waves of steepness less than 1/30 steepness across all tested periods.
- Wave overtopping loads are a contributing factor to divergence between linear forces and first harmonic CFD forces seen in all 1/15 numerical cases.
- Second order harmonic wave loads increase with incident wave steepness and are prominent in all 1/15 cases.
- Second harmonic force contributions carry greater significance for waves with shorter periods.

The presented work points to the considerable importance of 2^{nd} order harmonic loads and overtopping in reducing linear theory's capacity to model wave-structure interactions for the given WEC buoy section, both in terms of force predictions at high steepness and response estimations at wave periods close to the natural period. It is therefore suggested that when using linear potential software for analysis of similar designs, predictions should be made regarding the likelihood of overtopping as an indication of uncertainty in the model. Such software should be avoided if 2^{nd} order harmonic loads are of concern for structural integrity and resonant behaviour. Under steep wave conditions, OpenFOAM has proved to be an effective tool for modelling non-linear wave forces and overtopping when compared to experimental results, however using finer meshes is suggested for improved agreement.

8 FURTHER WORK

Provided here are suggestions to extend and benefit the presented project.

Analytical work could be expanded to include additional wave steepness, runs at 1/20 and 1/10 could provide greater detail of linear theory's capability to model wave-structure interactions for the given geometry.

Development of an indicator for the likelihood of overtopping would complement the work. One possible solution is to use linear theory and find a relation between structural freeboard, incident wave height and diffracted wave height to predict overtopping.

Comparison between the linear forces and responses calculated here with values computed using a linear BEM code for the given geometry would be of considerable interest in evaluating the methodology described in sections 5.2 & 5.4.

A validity study of the floating numerical simulations using experiments could be used to examine confidence in the presented response results. It would also be interesting to simulate the same wave cases but with the full cylindrical structure in 3D such that the applicability of 2D results could be examined.

REFERENCES

AGAMLOH, E. B., WALLACE, A. K. & VON JOUANNE, A. 2008. Application of fluid–structure interaction simulation of an ocean wave energy extraction device. *Renewable Energy,* 33**,** 748-757.

BAI, W. & TAYLOR, R. E. 2006. Higher-order boundary element simulation of fully nonlinear wave radiation by oscillating vertical cylinders. *Applied Ocean Research,* 28**,** 247-265.

CHEN, L., ZANG, J., HILLIS, A., MORGAN, G. & PLUMMER, A. 2014. Numerical investigation of wave–structure interaction using OpenFOAM. *Ocean Engineering,* 88**,** 91-109.

CRUZ, J. & SALTER, S. H. 2006. Numerical and experimental modelling of a modified version of the Edinburgh Duck wave energy device. *Proceedings of the Institution of Mechanical Engineers, Part M: Journal of Engineering for the Maritime Environment,* 220**,** 129-147.

DEAN, R. G. & DALRYMPLE, R. A. 1991. *Water wave mechanics for engineers and scientists*, World Scientific Publishing Co Inc.

DIZ-LOIS PALOMARES, G. 2015. CFD Simulations on a partially submerged cylinder under regular waves using OpenFOAM.

ELHANAFI, A. 2016. Prediction of regular wave loads on a fixed offshore oscillating water column-wave energy converter using CFD. *Journal of Ocean Engineering and Science,* 1**,** 268-283.

FALTINSEN, O. 1993. *Sea loads on ships and offshore structures*, Cambridge university press.

FERRANT, P., TOUZÉ, D. L. & PELLETIER, K. 2003. Non-linear time-domain models for irregular wave diffraction about offshore structures. *International journal for numerical methods in fluids*, 43**,** 1257-1277.

FOLLEY, M. 2016. *Numerical Modelling of Wave Energy Converters: State-of-the-Art Techniques for Single Devices and Arrays*, Academic Press.

HENRY, A., SCHMITT, P., WHITTAKER, T., RAFIEE, A. & DIAS, F. The characteristics of wave impacts on an oscillating wave surge converter. The Twenty-third International Offshore and Polar Engineering Conference, 2013. International Society of Offshore and Polar Engineers.

HIGUERA, P., LARA, J. L. & LOSADA, I. J. 2013. Realistic wave generation and active wave absorption for Navier–Stokes models: Application to OpenFOAM®. *Coastal Engineering,* 71**,** 102-118.

HUGHES, S. A. 1993. *Physical models and laboratory techniques in coastal engineering*, World Scientific.

HÄNNINEN, S. K., MIKKOLA, T. & MATUSIAK, J. 2016. Development of vertical second harmonic wave loads of a large cruise ship in short and steep head waves. *Ocean Engineering,* 118**,** 17-27.

ITURRIOZ, A., GUANCHE, R., LARA, J., VIDAL, C. & LOSADA, I. 2015. Validation of OpenFOAM® for oscillating water column three-dimensional modeling. *Ocean Engineering,* 107**,** 222-236.

KIM, M.-H. 1991. Nonlinear wave loads on fixed bodies:(comparison of second-order computation with experimental data). *Applied ocean research,* 13**,** 262-266.

LE MEHAUTE, B. 2013. *An introduction to hydrodynamics and water waves,* Springer Science & Business Media.

LE MÉHAUTÉ, B. An introduction to hydrodynamics and water waves. Oceanic Fronts in Coastal Processes, 1969. 114.

MCCABE, A., STALLARD, T., BAKER, N. & YAVUZ, H. 2007. Estimation of the responses of axisymmetric bodies in spread irregular waves. *Ocean engineering,* 34**,** 1371-1382.

MORGAN, G. & ZANG, J. 2011. Application of OpenFOAM to coastal and offshore modelling. *The 26th IWWWFB. Athens, Greece*.

MORGAN, G. C. J., ZANG, J., GREAVES, D., HEATH, A., WHITLOW, C. & YOUNG, J. 2011. Using the rasInterFoam CFD model for wave transformation and coastal modelling. *Coastal Engineering Proceedings,* 1**,** 23.

NEMATBAKHSH, A., BACHYNSKI, E. E., GAO, Z. & MOAN, T. 2015. Comparison of wave load effects on a TLP wind turbine by using computational fluid dynamics and potential flow theory approaches. *Applied Ocean Research,* 53**,** 142-154.

NEWMAN, J. 1996. The second-order wave force on a vertical cylinder. *Journal of Fluid Mechanics,* 320**,** 417-443.

PAULSEN, B. T., BREDMOSE, H., BINGHAM, H. B. & JACOBSEN, N. G. 2014. Forcing of a bottom-mounted circular cylinder by steep regular water waves at finite depth. *Journal of fluid mechanics,* 755**,** 1-34.

SCHMITT, P., BOURDIER, S., WHITTAKER, T., SARKAR, D., RENZI, E., DIAS, F., DOHERTY, K. & VAN'T HOFF, J. Hydrodynamic loading on a bottom hinged oscillating wave surge converter. The Twenty-second International Offshore and Polar Engineering Conference, 2012. International Society of Offshore and Polar Engineers.

SCHMITT, P. & ELSAESSER, B. 2015. On the use of OpenFOAM to model oscillating wave surge converters. *Ocean Engineering,* 108**,** 98-104.

SRINIVASAN, C., GAURAV, G., SERINO, G. & MIRANDA, S. 2011. Ringing and springing response of triangular TLPs. *International Shipbuilding Progress,* 58**,** 141-163.

YE LI & YI-HSIANG YU 2012. A Synthesis of Numerical Methods for Modeling Wave Energy Converter Point Absorbers. *Renewable and Sustainable Energy Reviews*.

YU, Y.-H. & LI, Y. A RANS simulation of the heave response of a two-body floating-point wave absorber. The Twenty-first International Offshore and Polar Engineering Conference, 2011. International Society of Offshore and Polar Engineers.

ZHAO, X.-Z., HU, C.-H. & SUN, Z.-C. 2010. Numerical simulation of extreme wave generation using VOF method. *Journal of Hydrodynamics, Ser. B,* 22**,** 466-477.